10 Nucleon matrix elements

Authors: S. Collins, R. Gupta, A. Nicholson, H. Wittig

A large number of experiments testing the Standard Model (SM) and searching for physics Beyond the Standard Model (BSM) involve either free nucleons (proton and neutron beams) or the scattering of electrons, protons, neutrinos and dark matter off nuclear targets. Necessary ingredients in the analysis of the experimental results are the matrix elements of various probes (fundamental currents or operators in a low energy effective theory) between nucleon or nuclear states. The goal of lattice-QCD calculations in this context is to provide high precision predictions of these matrix elements, the simplest of which give the nucleon charges and form factors. Determinations of the charges are the most mature and in this review we summarize the results for six quantities, the isovector and flavour diagonal axial vector, scalar and tensor charges. Other quantities that are not being reviewed but for which significant progress has been made in the last five years are the nucleon axial vector and electromagnetic form factors [1–9] and parton distribution functions [10]. The more challenging calculations of nuclear matrix elements, that are needed, for example, to calculate the cross-sections of neutrinos or dark matter scattering off nuclear targets, are proceeding along three paths. First is direct evaluation of matrix elements calculated with initial and final states consisting of multiple nucleons [11, 12]. Second, convoluting nucleon matrix elements with nuclear effects [13], and third, determining two and higher body terms in the nuclear potential via the direct or the HAL QCD methods [14, 15]. We expect future FLAG reviews to include results on these quantities once a sufficient level of control over all the systematics is reached.

10.1 Isovector and flavour diagonal charges of the nucleon

The simplest nucleon matrix elements are composed of local quark bilinear operators, $\overline{q_i}\Gamma_\alpha q_j$, where Γ_α can be any of the sixteen Dirac matrices. In this report, we consider two types of flavour structures: (a) when $i = u$ and $j = d$. These $\overline{u}\Gamma_\alpha d$ operators arise in $W^\pm$ mediated weak interactions such as in neutron or pion decay. We restrict the discussion to the matrix elements of the axial vector (A), scalar (S) and tensor (T) currents, which give the isovector charges, $g^{u-d}_{A,S,T}$.[1] (b) When $i = j$ for $j \in \{u, d, s, c\}$, there is no change of flavour, e.g., in processes mediated via the electromagnetic or weak neutral interaction or dark matter. These γ or Z^0 or dark matter mediated processes couple to all flavours with their corresponding charges. Since these probes interact with nucleons within nuclear targets, one has to include the effects of QCD (to go from the couplings defined at the quark and gluon level to those for nucleons) and nuclear forces in order to make contact with experiments. The isovector and flavour diagonal charges, given by the matrix elements of the corresponding operators calculated between nucleon states, are these nucleon level couplings. Here we review results for the light and strange flavours, $g^u_{A,S,T}$, $g^d_{A,S,T}$, and $g^s_{A,S,T}$.

The isovector and flavour diagonal operators also arise in BSM theories due to the exchange of novel force carriers or as effective interactions due to loop effects. The associated couplings are defined at the energy scale $\Lambda_{\rm BSM}$, while lattice-QCD calculations of matrix elements are carried out at a hadronic scale, μ, of a few GeV. The tool for connecting the couplings at

[1] In the isospin symmetric limit $\langle p|\bar{u}\Gamma d|n\rangle = \langle p|\bar{u}\Gamma u - \bar{d}\Gamma d|p\rangle = \langle n|\bar{d}\Gamma d - \bar{u}\Gamma u|n\rangle$ for nucleon and proton states $|p\rangle$ and $|n\rangle$, respectively. The latter two (equivalent) isovector matrix elements are computed on the lattice.

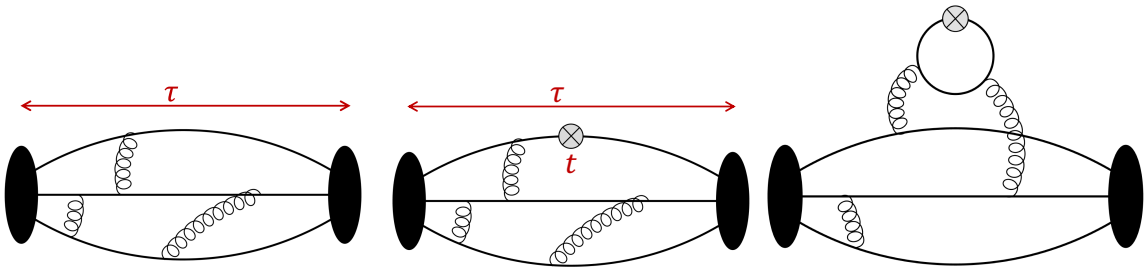

Figure 39: The two- and three-point correlation functions (illustrated by Feynman diagrams) that need to be calculated to extract the ground state nucleon matrix elements. (Left) the nucleon two-point function. (Middle) the connected three-point function with source-sink separation τ and operator insertion time slice t. (Right) the disconnected three-point function with operator insertion at t.

the two scales is the renormalization group. Since the operators of interest are composed of quark fields (and more generally also of gluon fields), the predominant change in the corresponding couplings under a scale transformation is due to QCD. To define the operators and their couplings at the hadronic scale μ, one constructs renormalized operators, whose matrix elements are finite in the continuum limit. This requires calculating both multiplicative renormalization factors, including the anomalous dimensions and finite terms, and the mixing with other operators. We discuss the details of the renormalization factors needed for each of the six operators reviewed in this report in Sec. 10.1.3.

Once renormalized operators are defined, the matrix elements of interest are extracted using expectation values of two-point and three-point correlation functions illustrated in Fig. 39, where the latter can have both quark line connected and disconnected contributions. In order to isolate the ground state matrix element, these correlation functions are analyzed using their spectral decomposition. The current practice is to fit the n-point correlation functions (or ratios involving three- and two-point functions) including contributions from one or two excited states.

The ideal situation occurs if the time separation τ between the nucleon source and sink positions, and the distance of the operator insertion time from the source and the sink, t and $\tau - t$, respectively, are large enough such that the contribution of all excited states is negligible. In the limit of large τ, the ratio of noise to signal in the nucleon two and three-point correlation functions grows exponentially as $e^{(M_N - \frac{3}{2}M_\pi)\tau}$ [16, 17], where M_N and M_π are the masses of the nucleon and the pion, respectively. Therefore, in particular at small pion masses, maintaining reasonable errors for large τ is challenging, with current calculations limited to $\tau \lesssim 1.5$ fm. In addition, the mass gap between the ground and excited (including multi-particle) states is smaller than in the meson sector and at these separations, excited-state effects can be significant. The approach commonly taken is to first obtain results with high statistics at multiple values of τ, using the methods described in Sec. 10.1.1. Then, as mentioned above, excited-state contamination is removed by fitting the data using a fit form involving one or two excited states. The different strategies that have been employed to minimize excited-state contamination are discussed in Sec. 10.1.2.

Usually, the quark-connected part of the three-point function (corresponding to the plot in the centre of Fig. 39) is computed via the so-called "sequential propagator method", which

uses the product of two quark propagators between the positions of the initial and the final nucleons as a source term for another inversion of the lattice Dirac operator. This implies that the position of the sink timeslice is fixed at some chosen value. Varying the value of the source-sink separation τ then requires the calculation of another sequential propagator.

The evaluation of quark-disconnected contributions is computationally more challenging as the disconnected loop (which contains the operator insertion, as illustrated in Fig. 39 right) is needed at all points on a particular timeslice or, in general, over the whole lattice. The quark loop is computed stochastically and then correlated with the nucleon two-point function before averaging this three-point function over the ensemble of gauge configurations. The associated statistical error, therefore, is a combination of that due to the stochastic evaluation (on each configuration) and that from the gauge average. The number of stochastic sources employed on each configuration is, typically, optimized to reduce the overall error for a given computational cost. The statistical errors of the connected contributions, in contrast, usually come only from the ensemble average since they are often evaluated exactly on each configuration, for a small number of source positions. If these positions are well-separated in space and time, then each measurement is statistically independent. The methodology applied for these calculations and the variance reduction techniques are summarized in Sec. 10.1.1. By construction, arbitrary values of τ across the entire temporal extent of the lattice can be realized when computing the quark-disconnected contribution, since the source-sink separation is determined by the part of the diagram that corresponds to the two-point nucleon correlator. However, in practice statistical fluctuations of both the connected and disconnected contributions increase sharply, so that the signal is lost in the statistical noise for $\tau \gtrsim 1.5\,\text{fm}$.

The lattice calculation is performed for a given number of quark flavours and at a number of values of the lattice spacing a, the pion mass M_π, and the lattice size, represented by $M_\pi L$. The results need to be extrapolated to the physical point defined by $a = 0$, $M_\pi = 135$ MeV and $M_\pi L \to \infty$. This is done by fitting the data simultaneously in these three variables using a theoretically motivated ansatz. The ansätze used and the fitting strategy are described in Sec. 10.1.4.

The procedure for rating the various calculations and the criteria specific to this chapter are discussed in Sec. 10.2, which also includes a brief description of how the final averages are constructed. The physics motivation for computing the isovector charges, $g_{A,S,T}^{u-d}$, and the review of the lattice results are presented in Sec. 10.3. This is followed by a discussion of the relevance of the flavour diagonal charges, $g_{A,S,T}^{u,d,s}$, and a presentation of the lattice results in Sec. 10.4.

10.1.1 Technical aspects of the calculations of nucleon matrix elements

The calculation of n-point functions needed to extract nucleon matrix elements requires making four essential choices. The first involves choosing between the suite of background gauge field ensembles one has access to. The range of lattice parameters should be large enough to facilitate the extrapolation to the continuum and infinite-volume limits, and the evaluation at the physical pion mass taken to be $M_\pi = 135$ MeV. Such ensembles have been generated with a variety of discretization schemes for the gauge and fermion actions that have different levels of improvement and preservation of continuum symmetries. The actions employed at present include (i) Wilson gauge with nonperturbatively improved Sheikholeslami-Wohlert fermions (nonperturbatively improved clover fermions) [18–24], (ii) Iwasaki gauge with nonperturbatively improved clover fermions [9, 25], (iii) Iwasaki gauge with twisted mass fermions

with a clover term [26–30], (iv) tadpole Symanzik improved gauge with highly improved staggered quarks (HISQ) [31–39], (v) Iwasaki gauge with domain wall fermions (DW) [40–46] and (vi) Iwasaki gauge with overlap fermions [47–49]. For details of the lattice actions, see Glossary A.1.

The second choice is of the valence quark action. Here there are two choices, to maintain a unitary formulation by choosing exactly the same action as is used in the generation of gauge configurations or to choose a different action and tune the quark masses to match the pseudoscalar meson spectrum in the two theories. Such mixed action formulations are nonunitary but are expected to have the same continuum limit as QCD. The reason for choosing a mixed action approach is expediency. For example, the generation of 2+1+1 flavour HISQ and 2+1 flavour DW ensembles with physical quark masses has been possible even at the coarse lattice spacing of $a = 0.15$ fm and there are indications that cut-off effects are reasonably small. These ensembles have been analyzed using clover-improved Wilson fermions, DW and overlap fermions since the construction of baryon correlation functions with definite spin and parity is much simpler compared to staggered fermions.

The third choice is the combination of the algorithm for inverting the Dirac matrix and variance reduction techniques. Efficient inversion and variance reduction techniques are needed for the calculation of nucleon correlation functions with high precision because the signal to noise degrades exponentially as $e^{(\frac{3}{2}M_\pi - M_N)\tau}$ with the source-sink separation τ. Thus, the number of measurements needed for high precision is much larger than in the meson sector. Commonly used inversion algorithms include the multigrid [50] and the deflation-accelerated Krylov solvers [51], which can handle linear systems with large condition numbers very efficiently, thereby enabling calculations of correlation functions at the physical pion mass.

The sampling of the path integral is limited by the number $N_{\rm conf}$ of gauge configurations generated. One requires sufficiently large $N_{\rm conf}$ such that the phase space (for example, different topological sectors) has been adequately sampled and all the correlation functions satisfy the expected lattice symmetries such as C, P, T, momentum and translation invariance. Thus, one needs gauge field generation algorithms that give decorrelated large volume configurations cost-effectively. On such large lattices, to reduce errors one can exploit the fact that the volume is large enough to allow multiple measurements of nucleon correlation functions that are essentially statistically independent. Two other common variance reduction techniques that reduce the cost of multiple measurements on each configuration are: the truncated solver with bias correction method [52] and deflation of the Dirac matrix for the low lying modes followed by sloppy solution with bias correction for the residual matrix consisting predominately of the high frequency modes [52, 53].

A number of other variation reduction methods are also being used and developed. These include deflation with hierarchical probing for disconnected diagrams [54, 55], the coherent source sequential propagator method [56, 57], low mode averaging [58, 59], the hopping parameter expansion [60, 61] and partitioning [62] (also known as dilution [63]).

The final choice is of the interpolating operator used to create and annihilate the nucleon state, and of the operator used to calculate the matrix element. Along with the choice of the interpolating operator (or operators if a variational method is used) one also chooses a "smearing" of the source used to construct the quark propagator. By tuning the width of the smearing, one can optimize the spatial extent of the nucleon interpolating operator to reduce the overlap with the excited states. Two common smearing algorithms are Gaussian (Wuppertal) [64] and Jacobi [65] smearing.

Having made all the above choices, for which a reasonable recipe exists, one calculates a statistical sample of correlation functions from which the desired ground state nucleon matrix element is extracted. Excited states, unfortunately, contribute significantly to nucleon correlation functions in present studies. To remove their contributions, calculations are performed with multiple source-sink separations τ and fits are made to the correlation functions using their spectral decomposition as discussed in the next section.

10.1.2 Controlling excited-state contamination

Nucleon matrix elements are determined from a combination of two- and three-point correlation functions. To be more specific, let $B^\alpha(\vec{x},t)$ denote an interpolating operator for the nucleon. Placing the initial state at timeslice $t=0$, the two-point correlation function of a nucleon with momentum $\vec{p}$ reads

$$C_2(\vec{p};\tau) = \sum_{\vec{x},\vec{y}} e^{i\vec{p}\cdot(\vec{x}-\vec{y})}\, \mathbb{P}_{\beta\alpha} \left\langle B^\alpha(\vec{x},\tau)\, \overline{B}^\beta(\vec{y},0) \right\rangle, \tag{360}$$

where the projector $\mathbb{P}$ selects the polarization, and α,β denote Dirac indices. The three-point function of two nucleons and a quark bilinear operator O_Γ is defined as

$$C_3^\Gamma(\vec{q};t,\tau) = \sum_{\vec{x},\vec{y},\vec{z}} e^{i\vec{p}'\cdot(\vec{x}-\vec{z})}\, e^{-i\vec{p}\cdot(\vec{y}-\vec{z})}\, \mathbb{P}_{\beta\alpha} \left\langle B^\alpha(\vec{x},\tau)\, O_\Gamma(\vec{z},t)\, \overline{B}^\beta(\vec{y},0) \right\rangle, \tag{361}$$

where $\vec{p}$, $\vec{p}\,'$ denote the momenta of the nucleons at the source and sink, respectively, and $\vec{q}\equiv\vec{p}\,'-\vec{p}$ is the momentum transfer. The bilinear operator is inserted at timeslice t, and τ denotes the source-sink separation. Both C_2 and C_3^Γ are constructed using the nonperturbative quark propagators, $D^{-1}(y,x)$, where D is the lattice Dirac operator.

The framework for the analysis of excited-state contamination is based on spectral decomposition. After inserting complete sets of eigenstates of the transfer matrix, the expressions for the correlators C_2 and C_3^Γ read

$$C_2(\vec{p};\tau) = \frac{1}{L^3}\sum_n \mathbb{P}_{\beta\alpha}\, \langle\Omega|B^\alpha|n\rangle\langle n|\overline{B}^\beta|\Omega\rangle\, e^{-E_n\tau}, \tag{362}$$

$$C_3^\Gamma(\vec{q};t,\tau) = \frac{1}{L^3}\sum_{n,m} \mathbb{P}_{\beta\alpha}\, \langle\Omega|B^\alpha|n\rangle\, \langle n|O_\Gamma|m\rangle\, \langle m|\overline{B}^\beta|\Omega\rangle\, e^{-E_n(\tau-t)}\, e^{-E_m t}, \tag{363}$$

where $|\Omega\rangle$ denotes the vacuum state, and E_n represents the energy of the n^{th} eigenstate $|n\rangle$ in the nucleon channel. Here we restrict the discussion to vanishing momentum transfer, $\vec{q}=0$ and label the ground state by $n=0$. The matrix element of interest, $g_\Gamma \equiv \langle 0|O_\Gamma|0\rangle$ can, for instance, be obtained from the asymptotic behaviour of the ratio

$$R_\Gamma(t,\tau) \equiv \frac{C_3^\Gamma(\vec{q}=0;t,\tau)}{C_2(\vec{p}=0;\tau)} \overset{t,(\tau-t)\to\infty}{\longrightarrow} g_\Gamma + \mathrm{O}(e^{-\Delta t},\, e^{-\Delta(\tau-t)},\, e^{-\Delta\tau}), \tag{364}$$

where $\Delta \equiv E_1 - E_0$ denotes the energy gap between the ground state and the first excitation. Here we assume that the bilinear operator O_Γ is appropriately renormalized (see Sec. 10.1.3).

Excited states with the same quantum numbers as the nucleon include resonances such as a Roper-like state with a mass of about 1.5 GeV, or multi-particle states consisting of a

nucleon and one or more pions [66, 67]. The latter are expected to be responsible for the most relevant sub-leading contributions to two- and three-point correlators in Eqs. (358) and (359) or their ratios (362) as the pion mass approaches its physical value. Ignoring the interactions between the individual hadrons, one can easily identify the lowest-lying multi-particle states: they include the $N\pi\pi$ state with all three particles at rest at $\sim 1.2\,\mathrm{GeV}$, as well as $N\pi$ states with both hadrons having nonzero and opposite momentum. Depending on the spatial box size L in physical units (with the smallest nonzero momentum equal to $2\pi/L$), there may be a dense spectrum of $N\pi$ states before the first nucleon resonance is encountered. Corrections to nucleon correlation functions due to the pion continuum have been studied using chiral effective theory [66–69] and Lüscher's finite-volume quantization condition [70].

The well-known noise problem of baryonic correlation functions implies that the long-distance regime, $t, (\tau - t) \to \infty$, where the correlators are dominated by the ground state, is difficult to reach. Current lattice calculations of baryonic three-point functions are typically confined to source-sink separations of $\tau \lesssim 1.5\,\mathrm{fm}$, despite the availability of efficient noise reduction methods. In view of the dense excitation spectrum encountered in the nucleon channel, one has to demonstrate that the contributions from excited states are sufficiently suppressed to guarantee an unbiased determination of nucleon matrix elements. There are several strategies to address this problem:

- Multi-state fits to correlator ratios or individual two- and three-point functions;
- Three-point correlation functions summed over the operator insertion time t;
- Increasing the projection of the interpolator B^α onto the ground state.

The first of the above methods includes excited state contributions explicitly when fitting to the spectral decomposition of the correlation functions, Eqs. (360, 361) or, alternatively, their ratio (see Eq. (362)). In its simplest form, the resulting expression for R_Γ includes the contributions from the first excited state, i.e.,

$$R_\Gamma(t,\tau) = g_\Gamma + c_{01}\, e^{-\Delta t} + c_{10}\, e^{-\Delta(\tau-t)} + c_{11}\, e^{-\Delta\tau} + \ldots, \tag{365}$$

where c_{01}, c_{10}, c_{11} and Δ are treated as additional parameters when fitting $R_\Gamma(t,\tau)$ simultaneously over intervals in the source-sink separation τ and the operator insertion timeslice t. Multi-exponential fits become more difficult to stabilize for a growing number of excited states, since an increasing number of free parameters must be sufficiently constrained by the data. Therefore, a high level of statistical precision at several source-sink separations is required. One common way to address this issue is to introduce Bayesian constraints, as described in [71]. Alternatively, one may try to reduce the number of free parameters by fixing the energy gap Δ (see, for instance, Ref. [2]), by assuming that the lowest-lying excitations are described by noninteracting multi-particle states consisting of the nucleon and at least one pion.

Ignoring the explicit contributions from excited states and fitting $R_\Gamma(t,\tau)$ to a constant in t for fixed τ amounts to applying what is called the "plateau method". The name derives from the ideal situation that sufficiently large source-sink separations τ can be realized, which would cause $R_\Gamma(t,\tau)$ to exhibit a plateau in t independent of τ. The ability to control excited-state contamination is rather limited in this approach, since the only option is to check for consistency in the estimate of the plateau as τ is varied. In view of the exponential degradation of the statistical signal for increasing τ, such stability checks are difficult to perform reliably.

Summed operator insertions, originally proposed in Ref. [72], have also emerged as a widely used method to address the problem of excited state contamination. One way to implement this method [73, 74] proceeds by summing $R_\Gamma(t,\tau)$ over the insertion time t, resulting in the correlator ratio $S_\Gamma(\tau)$,

$$S_\Gamma(\tau) \equiv \sum_{t=a}^{\tau-a} R_\Gamma(t,\tau). \tag{366}$$

The asymptotic behaviour of $S_\Gamma(\tau)$, including sub-leading terms, for large source-sink separations τ can be easily derived from the spectral decomposition of the correlators and is given by [75]

$$S_\Gamma(\tau) \overset{\tau\gg 1/\Delta}{\longrightarrow} K_\Gamma + (\tau-a)\, g_\Gamma + (\tau-a)\, e^{-\Delta\tau} d_\Gamma + e^{-\Delta\tau} f_\Gamma + \ldots, \tag{367}$$

where K_Γ is a constant, and the coefficients d_Γ and f_Γ contain linear combinations of transition matrix elements involving the ground and first excited states. Thus, the matrix element of interest, g_Γ, is obtained from the linear slope of $S_\Gamma(\tau)$ with respect to the source-sink separation τ. While the leading corrections from excited states are parametrically smaller than those of the original ratio $R_\Gamma(t,\tau)$ (see Eq. (362)), extracting the slope from a linear fit to $S_\Gamma(\tau)$ typically results in relatively large statistical errors. In principle, one could include the contributions from excited states explicitly in the expression for $S_\Gamma(\tau)$. However, in practice it is often difficult to constrain an enlarged set of parameters reliably, in particular if one cannot afford to determine $S_\Gamma(\tau)$ except for a handful of source-sink separations.

The original summed operator insertion technique described in Refs. [64, 72, 76, 77] avoids the explicit summation over the operator insertion time t at every fixed value of τ. Instead, one replaces one of the quark propagators that appear in the representation of the two-point correlation function $C_2(t)$ by a "sequential" propagator, according to

$$D^{-1}(y,x) \to D_\Gamma^{-1}(y,x) = \sum_z D^{-1}(y,z)\Gamma D^{-1}(z,x). \tag{368}$$

In this expression, the position $z \equiv (\vec{z},t)$ of the insertion of the quark bilinear operator is implicitly summed over, by inverting the lattice Dirac operator D on the source field $\Gamma D^{-1}(z,x)$. While this gives access to all source-sink separations $0 \le \tau \le T$, where T is the temporal extent of the lattice, the resulting correlator also contains contact terms, as well as contributions from $\tau < t < T$ that must be controlled. This method[2] has been adopted recently by the CalLat collaboration in their calculation of the isovector axial charge [35, 39].

As in the case of explicitly summing over the operator insertion time, the matrix element of interest is determined from the slope of the summed correlator. For instance, in Ref. [39], the axial charge was determined from the summed three-point correlation function, by fitting to its asymptotic behaviour [78] including sub-leading terms.

In practice, one often uses several methods simultaneously [e.g., multi-state fits and the summation method based on Eq. (365)], in order to check whether the results converge towards a common value. All of the approaches for controlling excited-state contributions proceed by fitting data obtained in a finite interval in τ to a function that describes the approach to the asymptotic behaviour derived from the spectral decomposition. Obviously, the accessible values of τ must be large enough so that the model function provides a good representation

[2] In Ref. [78] it is shown that the method can be linked to the Feynman-Hellmann theorem. A direct implementation of the Feynman-Hellmann theorem by means of a modification of the lattice action is discussed and applied in Refs. [79, 80].

of the data that enter such a fit. It is then reasonable to impose a lower threshold on τ above which the fit model is deemed reliable. We will return to this issue when explaining our quality criteria in Sec. 10.2.

The third method for controlling excited-state contamination aims at optimizing the projection onto the ground state in the two-point and three-point correlation functions [22, 57, 81]. The RQCD collaboration has chosen to optimize the parameters in the Gaussian smearing procedure, so that the overlap of the nucleon interpolating operator onto the ground state is maximized [22]. In this way it may be possible to use shorter source-sink separations without incurring a bias due to excited states.

The variational method, originally designed to provide detailed information on energy levels of the ground and excited states in a given channel [82–85], has also been adapted to the determination of hadron-to-hadron transition elements [75]. In the case of nucleon matrix elements, the authors of Ref. [81] have employed a basis of operators to construct interpolators that couple to individual eigenstates in the nucleon channel. The method has produced promising results when applied to calculations of the axial and other forward matrix elements at a fixed value of the pion mass [57, 81, 86]. However, a more comprehensive study aimed at providing an estimate at the physical point has, until now, not been performed.

10.1.3 Renormalization and Symanzik improvement of local currents

In this section we discuss the matching of the normalization of lattice operators to a continuum reference scheme such as $\overline{\rm MS}$, and the application of Symanzik improvement to remove $O(a)$ contributions. The relevant operators for this review are the axial (A_μ), tensor ($T_{\mu\nu}$) and scalar (S) local operators of the form $\mathcal{O}_\Gamma = \overline{q}\Gamma q$, with $\Gamma = \gamma_\mu\gamma_5$, $i\sigma_{\mu\nu}$ and $\mathbf{1}$, respectively, whose matrix elements are evaluated in the forward limit. The general form for renormalized operators in the isovector flavour combination, at a scale μ, reads

$$\mathcal{O}_\Gamma^{\overline{\rm MS}}(\mu) = Z_{\mathcal{O}}^{\overline{\rm MS},{\rm Latt}}(\mu a, g^2)\left[\mathcal{O}_\Gamma(a) + ab_{\mathcal{O}} m\mathcal{O}_\Gamma(a) + ac_{\mathcal{O}}\mathcal{O}_\Gamma^{\rm imp}(a)\right] + O(a^2), \tag{369}$$

where $Z_{\mathcal{O}}^{\overline{\rm MS},{\rm Latt}}(\mu a, g^2)$ denotes the multiplicative renormalization factor determined in the chiral limit and the second and third terms represent all possible mass dependent and mass independent Symanzik improvement terms, respectively.[3] The chiral properties of overlap, domain-wall fermions (with improvement up to $O(m_{\rm res}^n)$ where $m_{\rm res}$ is the residual mass) and twisted mass fermions (at maximal twist [91, 92]) mean that the $O(a)$ improvement terms are absent, while for nonperturbatively improved Sheikholeslami-Wohlert-Wilson (nonperturbatively-improved clover) fermions all terms appear in principle. For the operators of interest here there are several mass dependent terms but at most one (higher dimensional) $\mathcal{O}_\Gamma^{\rm imp}$, see, e.g., Refs. [93, 94]. However, the latter involve external derivatives whose corresponding matrix elements vanish in the forward limit. Note that no mention is made of staggered fermions as they are not, currently, widely employed as valence quarks in nucleon matrix element calculations.

In order to illustrate the above remarks we consider the renormalization and improvement of the isovector axial current. This current has no anomalous dimension and hence the

[3] Here $a(g^2)$ refers to the lattice spacing in the chiral limit, however, lattice simulations are usually carried out by fixing the value of g^2 while varying the quark masses. This means $a = a(\tilde{g}^2)$ where $\tilde{g}^2 = g^2(1 + b_g a m_q)$ [87, 88] is the improved coupling that varies with the average sea-quark mass m_q. The difference between the Z factors calculated with respect to g^2 and $\tilde{g}^2$ can effectively be absorbed into the $b_{\mathcal{O}}$ coefficients [89, 90].

renormalization factor, $Z_A = Z_A^{\overline{\rm MS},{\rm Latt}}(g^2)$, is independent of the scale. The factor is usually computed nonperturbatively via the axial Ward identity [95] or the Rome-Southampton method [96] (see Sec. A.3 for details). In some studies, the ratio with the corresponding vector renormalization factor, Z_A/Z_V, is determined for which some of the systematics cancel. In this case, one constructs the combination $Z_A g_A/(Z_V g_V)$, where $Z_V g_V = 1$ and g_A and g_V are the lattice forward matrix elements, to arrive at the renormalized axial charge [34]. For domain wall fermions the ratio is employed in order to remove $O(am_{\rm res})$ terms and achieve leading discretisation effects starting at $O(a^2)$ [97]. Thus, as mentioned above, $O(a)$ improvement terms are only present for nonperturbatively-improved clover fermions. For the axial current, Eq. (367) takes the explicit form,

$$A_\mu^{\overline{\rm MS}}(\mu) = Z_A^{\overline{\rm MS},{\rm Latt}}(g^2)\left[\left(1 + ab_A m_{\rm val} + 3a\tilde{b}_A m_{\rm sea}\right) A_\mu(a) + ac_A \partial_\mu P(a)\right] + O(a^2), \quad (370)$$

where $m_{\rm val}$ and $m_{\rm sea}$ are the average valence- and sea-quark masses derived from the vector Ward identity [88, 94, 95], and P is the pseudoscalar operator $\overline{q}\gamma_5 q$. The matrix element of the derivative term is equivalent to $q_\mu \langle N(p')|P|N(p)\rangle$ and hence vanishes in the forward limit when the momentum transfer $q_\mu = 0$. The improvement coefficients b_A and $\tilde{b}_A$ are known perturbatively for a variety of gauge actions [93, 98, 99] and nonperturbatively for the tree-level Symanzik-improved gauge action for $N_f = 2 + 1$ [100].

Turning to operators for individual quark flavours, these can mix under renormalization and the singlet and nonsinglet renormalization factors can differ. For the axial current, such mixing occurs for all fermion formulations just like in the continuum, where the singlet combination acquires an anomalous dimension due to the $\mathrm{U}_A(1)$ anomaly. The ratio of singlet to nonsinglet renormalization factors, $r_{\mathcal{O}} = Z_{\mathcal{O}}^{\rm s.}/Z_{\mathcal{O}}^{\rm n.s.}$ for $\mathcal{O} = A$ differs from 1 at $O(\alpha_s^2)$ in perturbation theory (due to quark loops), suggesting that the mixing is a small effect. The nonperturbative determinations performed so far find $r_A \approx 1$ [5, 28], supporting this. For the tensor current the disconnected diagram vanishes in the continuum due to chirality and consequently on the lattice $r_T = 1$ holds for overlap and DW fermions (assuming $m_{\rm res} = 0$ for the latter). For twisted-mass and clover fermions the mixing is expected to be small with $r_T = 1 + O(\alpha_s^3)$ [101] and this is confirmed by the nonperturbative studies of Refs. [30, 102].

The scalar operators for the individual quark flavours, $\overline{q}q$, are relevant not only for the corresponding scalar charges, but also for the sigma terms, $\sigma_q = m_q\langle N|\overline{q}q|N\rangle$, when combined with the quark masses (m_q). For overlap and DW fermions $r_S = 1$, like in the continuum and all $\overline{q}q$ renormalize multiplicatively with the isovector Z_S. The latter is equal to the inverse of the mass renormaliation and hence $m_q\overline{q}q$ is renormalization group (RG) invariant. For twisted mass fermions, through the use of Osterwalder-Seiler valence fermions, the operators $m_{ud}(\overline{u}u + \overline{d}d)$ and $m_s\overline{s}s$ are also invariant [103].[4] In contrast, the lack of good chiral properties leads to significant mixing between quark flavours for clover fermions. Nonperturbative determinations via the axial Ward identity [23, 104] have found the ratio r_S to be much larger than the perturbative expectation $1 + O(\alpha_s^2)$ [101] may suggest. While the sum over the quark flavours which appear in the action, $\sum_q^{N_f} m_q\overline{q}q$, is RG invariant, large cancellations between the contributions from individual flavours can occur when evaluating, e.g., the strange sigma term. Note that for twisted mass and clover fermions there is also an additive contribution

[4] Note that for twisted mass fermions the pseudoscalar renormalization factor is the relevant factor for the scalar operator. The isovector (isosinglet) scalar current in the physical basis becomes the isosinglet (isovector) pseudoscalar current in the twisted basis. Perturbatively $r_P = 1 + O(\alpha_s^3)$ and nonperturbative determinations have found $r_P \approx 1$ [30].

$\propto a^{-3}\mathbf{1}$ (or $\propto \mu a^{-2}\mathbf{1}$) to the scalar operator. This contribution is removed from the nucleon scalar matrix elements by working with the subtracted current, $\overline{q}q - \langle\overline{q}q\rangle$, where $\langle\overline{q}q\rangle$ is the vacuum expectation value of the current [94].

Symanzik improvement for the singlet currents follows the same pattern as in the isovector case with $O(a)$ terms only appearing for nonperturbatively-improved clover fermions. For the axial and tensor operators only mass dependent terms are relevant in the forward limit while for the scalar there is an additional gluonic operator $\mathcal{O}_S^{\rm imp} = \mathrm{Tr}(F_{\mu\nu}F_{\mu\nu})$ with a coefficient of $O(\alpha_s)$ in perturbation theory. When constructing the sigma terms from the quark masses and the scalar operator, the improvement terms remain and they must be included to remove all $O(a)$ effects for nonperturbatively-improved clover fermions, see Ref. [94] for a discussion.

10.1.4 Extrapolations in a, M_π and $M_\pi L$

To obtain physical results which can be used to compare to or make predictions for experiment, all quantities must be extrapolated to the continuum and infinite-volume limits. In general, either a chiral extrapolation or interpolation must also be made to the physical pion mass. These extrapolations need to be performed simultaneously since discretization and finite-volume effects are themselves dependent upon the pion mass. Furthermore, in practice it is not possible to hold the pion mass fixed while the lattice spacing is varied, as some variation in a occurs when tuning the quark masses at fixed gauge coupling. Thus, one performs a simultaneous extrapolation in all three variables using a theoretically motivated formula of the form,

$$g(M_\pi, a, L) = g_{\rm phys} + \delta_{M_\pi} + \delta_a + \delta_L \ , \tag{371}$$

where $g_{\rm phys}$ is the desired extrapolated result, and δ_{M_π}, δ_a, δ_L are the deviations due to the pion mass, the lattice spacing, and the volume, respectively. Below we outline the forms for each of these terms.

All observables discussed in this section are dimensionless, therefore the extrapolation formulae may be parameterized by a set of dimensionless variables:

$$\epsilon_\pi = \frac{M_\pi}{\Lambda_\chi} \ , \qquad M_\pi L \ , \qquad \epsilon_a = \Lambda_a a \ . \tag{372}$$

Here, $\Lambda_\chi \sim 1$ GeV is a chiral symmetry breaking scale, which, for example, can be set to $\Lambda_\chi = 4\pi F_\pi$, where $F_\pi = 92.2$ MeV is the pion decay constant, and Λ_a is a discretization scale, e.g., $\Lambda_a = \frac{1}{4\pi w_0}$, where w_0 is a gradient-flow scale [105].

Effective field theory methods may be used to determine the form of each of these extrapolations. For the single nucleon charges, Heavy-Baryon χPT (HBχPT) is a common choice [106], however, other formulations, such as unitarized χPT [107], are also employed. Various formulations of HBχPT exist, including those for two- and three-flavours, as well as with and without explicit Δ degrees of freedom. Two-flavour HBχPT is typically used due to issues with convergence of the three-flavour theory [25, 108–111]. The convergence properties of all known formulations for baryon χPT, even at the physical pion mass, have not been well-established, and are generally believed to be poor compared to purely mesonic χPT.

To $\mathcal{O}\left(\epsilon_\pi^2\right)$, the two-flavour chiral expansion for the nucleon charges is known to be of the form [112],

$$g = g_0 + g_1\epsilon_\pi + g_2\epsilon_\pi^2 + \tilde{g}_2\epsilon_\pi^2 \ln\left(\epsilon_\pi^2\right) \ , \tag{373}$$

where $g_1 = 0$ for all charges g except $g_S^{u,d}$. The dimensionless coefficients $g_{0,1,2}, \tilde{g}_2$ are assumed to be different for each of the different charges. The coefficients in front of the logarithms, $\tilde{g}_2$, are known functions of the lower order coefficients (LECs), and do not represent new, independent LECs. Mixed action calculations will have further dependence upon the mixed valence-sea pion mass, m_{vs}.

Given the potential difficulties with convergence of the chiral expansion, known values of the $\tilde{g}_2$ in terms of LECs are not typically used, but are left as free fit parameters. Furthermore, many quantities have been found to display mild pion mass dependence, such that Taylor expansions, i.e., neglecting logarithms in the above expressions, are also often employed. The lack of a rigorously established theoretical basis for the extrapolation in the pion mass thus requires data close to the physical pion mass for obtaining high precision extrapolated/interpolated results.

Discretization effects depend upon the lattice action used in a particular calculation, and their form may be determined using the standard Symanzik power counting. In general, for an unimproved action, the corrections due to discretization effects, δ_a, include terms of the form,

$$\delta_a = c_1 \epsilon_a + c_2 \epsilon_a^2 + \cdots \ , \tag{374}$$

where $c_{1,2}$ are dimensionless coefficients. Additional terms of the form $\tilde{c}_n \left(\epsilon_\pi \epsilon_a\right)^n$, where n is an integer whose lowest value depends on the combined discretization and chiral properties, will also appear. Improved actions systematically remove correction terms, e.g., an $\mathcal{O}\left(a\right)$ improved action, combined with an similarly improved operator, will contain terms in the extrapolation ansatz beginning at ϵ_a^2 (see Sec. 10.1.3).

Finite volume corrections, δ_L, may be determined in the usual way from effective field theory, by replacing loop integrals over continuous momenta with discrete sums. Finite volume effects therefore introduce no new undetermined parameters to the extrapolation. For example, at next-to-leading order, and neglecting contributions from intermediate delta baryons, the finite-volume corrections for the axial charge in two-flavour HBχPT take the form [113],

$$\delta_L \ \equiv \ g_A(L) - g_A(\infty) = \frac{8}{3}\epsilon_\pi^2 \left[g_0^3 F_1\left(M_\pi L\right) + g_0 F_3\left(M_\pi L\right) \right] \ , \tag{375}$$

where

$$\begin{aligned} F_1\left(mL\right) &= \sum_{\mathbf{n}\neq\mathbf{0}} \left[K_0\left(mL|\mathbf{n}|\right) - \frac{K_1\left(mL|\mathbf{n}|\right)}{mL|\mathbf{n}|} \right] \\ F_3\left(mL\right) &= -\frac{3}{2} \sum_{\mathbf{n}\neq 0} \frac{K_1\left(mL|\mathbf{n}|\right)}{mL|\mathbf{n}|} \ , \end{aligned} \tag{376}$$

and $K_\nu(z)$ are the modified Bessel functions of the second kind. Some extrapolations are performed using the form for asymptotically large $M_\pi L$,

$$K_0(z) \to \frac{e^{-z}}{\sqrt{z}} \ , \tag{377}$$

and neglecting contributions due to K_1. Care must, however, be taken to establish that these corrections are negligible for all included values of $M_\pi L$. The numerical coefficients, for

example, 8/3 in Eq. (373), are often taken to be additional free fit parameters, due to the question of convergence of the theory discussed above.

Given the lack of knowledge about the convergence of the expansions and the resulting plethora of possibilities for extrapolation models at differing orders, it is important to include statistical tests of model selection for a given set of data. Bayesian model averaging [114] or use of the Akaike Information Criterion [115] are common choices which penalize over-parameterized models.

10.2 Quality criteria for nucleon matrix elements and averaging procedure

There are two specific issues which call for a modification and extension of the FLAG quality criteria listed in Sec. 2. The first concerns the rating of the chiral extrapolation: The FLAG criteria reflect the ability of χPT to provide accurate descriptions of the pion mass dependence of observables. Clearly, this ability is linked to the convergence properties of χPT in a particular mass range. Quantities extracted from nucleon matrix elements are extrapolated to the physical pion mass using some variant of baryonic χPT, whose convergence is not as well established compared to the mesonic sector. Therefore, we have opted for stricter quality criteria concerning the chiral extrapolation of nucleon matrix elements, i.e.,

★ $M_{\pi,\min} < 200$ MeV with three or more pion masses used in the extrapolation
or two values of M_π with one lying within 10 MeV of 135 MeV (the physical neutral pion mass) and the other one below 200 MeV
○ 200 MeV $\leq M_{\pi,\min} \leq 300$ MeV with three or more pion masses used in the extrapolation;
or two values of M_π with $M_{\pi,\min} < 200$ MeV;
or a single value of M_π lying within 10 MeV of 135 MeV (the physical neutral pion mass)
■ Otherwise

In Sec. 10.1.2 we have discussed that insufficient control over excited state contributions, arising from the noise problem in baryonic correlation functions, may lead to a systematic bias in the determination of nucleon matrix elements. We therefore introduce an additional criterion that rates the efforts to suppress excited state contamination in the final result. As described in Sec. 10.1.2, the source-sink separation τ, i.e., the Euclidean distance between the initial and final nucleons, is the crucial variable. The rating scale concerning control over excited state contributions is thus

★ Three or more source-sink separations τ, at least two of which must be above 1.0 fm.
○ Two or more source-sink separations, τ, with at least one value above 1.0 fm.
■ Otherwise

Despite the enormous progress achieved in reducing excited state contamination, we emphasize that more stringent quality criteria may have to be adopted in future editions of the FLAG report to control this important systematic effect at the stated level of precision.

As explained in Sec. 2, FLAG averages are distinguished by the sea-quark content. Hence, for a given configuration of the quark sea (i.e., for $N_f = 2$, $2+1$ or $2+1+1$), we first identify those calculations that pass the FLAG and the additional quality criteria defined in this section, i.e., excluding any calculation that has a red tag in one or more of the categories. We

then add statistical and systematic errors in quadrature and perform a weighted average. If the fit is of bad quality (i.e., if $\chi^2_{\rm min}/{\rm dof} > 1$), the errors of the input quantities are scaled by $\sqrt{\chi^2/{\rm dof}}$. In the following step, correlations among different calculations are taken into account in the error estimate by applying Schmelling's procedure [116].

10.3 Isovector charges

The axial, scalar and tensor isovector charges are needed to interpret the results of many experiments and phenomena mediated by weak interactions, including probes of new physics. The most natural process from which isovector charges can be measured is neutron beta decay ($n \to p^+ e^- \overline{\nu}_e$). At the quark level, this process occurs when a down quark in a neutron transforms into an up quark due to weak interactions, in particular due to the axial current interaction. While scalar and tensor currents have not been observed in nature, effective scalar and tensor interactions arise in the SM due to loop effects. At the TeV and higher scales, contributions to these three currents could arise due to new interactions and/or loop effects in BSM theories. These super-weak corrections to standard weak decays can be probed through high precision measurements of the neutron decay distribution by examining deviations from SM predictions as described in Ref. [117]. The lattice-QCD methodology for the calculation of isovector charges is well-established, and the control over statistical and systematic uncertainties is becoming robust.

The axial charge g_A^{u-d} is an important parameter that encapsulates the strength of weak interactions of nucleons. It enters in many analyses of nucleon structure and of SM and BSM physics. For example, it enters in (i) the extraction of V_{ud} and tests of the unitarity of the Cabibbo-Kobayashi-Maskawa (CKM) matrix; (ii) the analysis of neutrinoless double-beta decay, (iii) neutrino-nucleus quasi-elastic scattering cross-section; (iv) the rate of proton-proton fusion, the first step in the thermonuclear reaction chains that power low-mass hydrogen-burning stars like the Sun; (v) solar and reactor neutrino fluxes; (vi) muon capture rates, etc.. The current best determination of the ratio of the axial to the vector charge, g_A/g_V, comes from measurement of neutron beta decay using polarized ultracold neutrons by the UCNA collaboration, 1.2772(20) [118, 119], and by PERKEO II, 1.2761^{+14}_{-17} [120]. Note that, in the SM, $g_V = 1$ up to second order corrections in isospin breaking [121, 122] as a result of the conservation of the vector current. Given the accuracy with which g_A^{u-d} has been measured in experiments, the goal of lattice-QCD calculations is to calculate it directly with $O(1\%)$ accuracy.

Isovector scalar or tensor interactions contribute to the helicity-flip parameters, called b and B, in the neutron decay distribution. By combining the calculation of the scalar and tensor charges with the measurements of b and B, one can put constraints on novel scalar and tensor interactions at the TeV scale as described in Ref. [117]. To optimally bound such scalar and tensor interactions using measurements of b and B parameters in planned experiments targeting 10^{-3} precision [123–125], we need to determine g_S^{u-d} and g_T^{u-d} at the 10% level as explained in Refs. [34, 117]. Future higher-precision measurements of b and B would require correspondingly higher-precision calculations of the matrix elements to place even more stringent bounds on these couplings at the TeV-scale.

One can estimate g_S^{u-d} using the conserved vector current (CVC) relation, $g_S/g_V = (M_N - M_P)^{\rm QCD}/(m_d - m_u)^{\rm QCD}$, as done by Gonzalez-Alonso *et al.* [126]. In their analysis, they took estimates of the two mass differences on the right-hand side from the global lattice-QCD data [127] and obtained $g_S^{u-d} = 1.02(8)(7)$.

The tensor charge g_T^{u-d} can be extracted experimentally from semi-inclusive deep-inelastic scattering (SIDIS) data [128–131]. A sample of these phenomenological estimates is shown in Fig. 42, and the noteworthy feature is that the current uncertainty in these estimates is large.

10.3.1 Results for g_A^{u-d}

Calculations of the isovector axial charge have a long history, as can be seen from the compilation given in Tab. 62 and plotted in Fig. 40. There are results in two-flavour QCD, as well as for QCD with $N_f = 2+1$ and $2+1+1$ dynamical flavours. All calculations discussed below use renormalization factors that were determined nonperturbatively, either via Ward identities or the Rome-Southampton method.

The issue of excited state contamination received little if any attention before 2010. As a consequence, the range of source-sink separations employed in many of the early calculations prior to that year was rather limited, offering little control over this important systematic effect. This concerns the calculations by LHPC 05 [134], LHPC 10 [56], RBC 08 [135], RBC/UKQCD 08 [40], RBC/UKQCD 09B [41] and QCDSF 06 [18].

The Mainz group has performed calculations in two-flavour QCD, based on the ensembles generated by the Coordinated Lattice Simulations (CLS) effort, using nonperturbatively improved Wilson fermions and the Wilson gauge action. In their first calculation (Mainz 12 [21]) they computed three-point correlators over several source-sink separations up to $\tau \approx 1.3\,\text{fm}$. By comparing the technique of summed operator insertions (the "summation method") to the more traditional plateau method, they found that the former gave consistently larger estimates for g_A^{u-d}, which were in better agreement with the experimental value. In a follow-up paper (Mainz 17 [24]) they added more statistics, extended the range of pion masses towards lower values and used two-state fits in addition to the summation method.

Two flavours of O(a) improved Wilson quarks were also used in the calculations performed by QCDSF 06 [18], QCDSF 13 [20] and RQCD 14 [22]. QCDSF 13 [20] is an extension of the earlier study QCDSF 06 [18], including ensembles at smaller lattice spacing. Control over excited-state effects is still limited, since a range of several source-sink separations was studied only on one ensemble, and the main result was derived from the plateau method at a single source-sink separation of about 1 fm. The calculation by the Regensburg group (RQCD 14 [22]) was performed on a large part of the same ensembles used by QCDSF 13, supplemented by a larger volume at the smallest pion mass of 150 MeV and by an additional ensemble at coarser lattice spacing with $M_\pi = 290\,\text{MeV}$. The strategy employed in RQCD 14 to control excited-state contamination was focused on optimizing the overlap of the nucleon interpolator onto the ground state, by choosing appropriate parameters in the smearing procedure. The efficacy of this approach was studied on a subset of ensembles for $\tau \sim 0.5 - 1.2\,\text{fm}$. In both QCDSF 13 and RQCD 14, the axial charge was determined from the ratio g_A/f_π in which finite-volume effects and other systematic errors are expected to cancel approximately.

The ETM collaboration has published results for the axial charge [26, 28], obtained using $N_f = 2$ flavours of twisted-mass Wilson fermions. In ETM 15D [26], three different source-sink separations were studied, and the range of pion masses was extended down to the physical values. The quoted result for g_A^{u-d} originates from a single lattice spacing and was obtained using the plateau method at the largest value of the source-sink separation τ where agreement with the summation method was found. A further extension of the analysis (ETM 17B [28]) was performed at a single (but almost physical) pion mass value and single lattice spacing.

Collaboration	Ref.	N_f	publication status	continuum extrapolation	chiral extrapolation	finite volume	renormalization	excited states	g_A^{u-d}
PNDME 18[a]	[38]	2+1+1	A	★‡	★	★	★	★	1.218(25)(30)
CalLat 18	[39]	2+1+1	A	○	★	★	★	★	1.271(10)(7)
CalLat 17	[35]	2+1+1	P	○	★	★	★	★	1.278(21)(26)
PNDME 16[a]	[34]	2+1+1	A	○‡	★	★	★	★	1.195(33)(20)
Mainz 18	[132]	2+1	C	★	○	★	★	★	1.251(24)
PACS 18	[9]	2+1	A	■	■	★	★	■	1.163(75)(14)
χQCD 18	[46]	2+1	A	○	★	★	★	★	1.254(16)(30)[$]
JLQCD 18	[49]	2+1	A	■	○	○	★	★	1.123(28)(29)(90)
LHPC 12A[b]	[133]	2+1	A	■‡	★	★	★	★	0.97(8)
LHPC 10	[56]	2+1	A	■	○	■	★	■	1.21(17)
RBC/UKQCD 09B	[41]	2+1	A	■	■	○	★	■	1.19(6)(4)
RBC/UKQCD 08B	[40]	2+1	A	■	■	○	★	■	1.20(6)(4)
LHPC 05	[134]	2+1	A	■	■	★	★	■	1.226(84)
Mainz 17	[24]	2	A	★	★	★	★	○	$1.278(68)(^{+0}_{-0.087})$
ETM 17B	[28]	2	A	■	○	○	★	★	1.212(33)(22)
ETM 15D	[26]	2	A	■	○	○	★	★	1.242(57)
RQCD 14	[22]	2	A	○	★	★	★	■	1.280(44)(46)
QCDSF 13	[20]	2	A	○	★	■	★	■	1.29(5)(3)
Mainz 12	[21]	2	A	★	○	○	★	○	$1.233(63)(^{+0.035}_{-0.060})$
RBC 08	[135]	2	A	■	■	■	★	■	1.23(12)
QCDSF 06	[18]	2	A	○	■	■	★	■	1.31(9)(7)

[a] The improvement coefficient in the valence quark action is set to its tadpole-improved tree-level value.
[b] The quark action is tree-level improved.
‡ The rating takes into account that the action is not fully O(a) improved by requiring an additional lattice spacing.
[$] For this partially quenched analysis the criteria are applied to the unitary points.

Table 62: Overview of results for g_A^{u-d}.

ETMC quote the result at the smallest source-sink separation τ for which the plateau value agrees with the two-state fit as their main estimate. Agreement with the summation method is also observed, albeit within the larger statistical errors of the latter.

Estimates for the axial charge with $N_f = 2 + 1$ have been published by the LHPC [56, 133, 134] and RBC/UKQCD collaborations [40, 41] and, more recently, by JLQCD 18 [49],

χQCD 18 [46], PACS 18 [9], and Mainz 18 [132].

The calculations in LHPC 05 [134] and LHPC 10 [56] were performed employing a mixed-action setup, combining domain wall fermions in the valence sector with staggered (Asqtad) gauge ensembles generated by MILC. Although the dependence of the results on the source-sink separation was studied to some extent in LHPC 10, excited state effects are not sufficiently controlled according to our quality criteria described in Sec. 10.2. A different discretization of the quark action was used in their later study (LHPC 12A [133]), based on tree-level improved Wilson fermions with smeared gauge links, both in the sea and valence sectors. While this setup does not realize full O(a) improvement, it was found that smeared gauge links reduce the leading discretization effects of O(a) substantially. Three source-sink separations were studied in LHPC 12A on each ensemble down to nearly the physical quark mass at a single value of the lattice spacing. The quoted estimate for the axial charge is uncharacteristically low. While other quantities determined in the same study agreed well with experiment or other groups, the reasons for such a low value of g_A^{u-d} could not be established.

The RBC/UKQCD collaboration has employed $N_f = 2{+}1$ flavours of domain wall fermions in their calculations. The results quoted in RBC/UKQCD 08B [40] and RBC/UKQCD 09B [41] were obtained at relatively heavy pion masses at a single value of the lattice spacing, with only limited control over excited state effects. A systematic investigation of different source-sink separations has only been performed more recently [136], however, without quoting an estimate for g_A^{u-d}.

The JLQCD collaboration JLQCD 18 [49] have performed a calculation using $N_f = 2 + 1$ flavours of overlap fermions and the Iwasaki gauge action. Owing to the large numerical cost of overlap fermions, which preserve exact chiral symmetry at nonzero lattice spacing, they have only simulated four light quark masses with $290 < M_\pi < 540$ MeV and at a single lattice spacing so far. Their simultaneous fit to the data for the correlator ratio $R_A(t, \tau)$ computed at six values of τ to a constant, gives a low value for g_A^{u-d} at the physical point. Overlap valence quarks were also used by the χQCD collaboration in their study of various nucleon matrix elements (χQCD 18 [46]), utilizing the gauge ensembles generated by RBC/UKQCD with domain wall fermions. The quoted estimate for the axial charge was obtained from a combination of two-state fits and the summation method, applied over a range of source-sink separations.

Two recent calculations with $N_f = 2 + 1$ have used O(a) improved Wilson fermions. The focus of the study by the PACS collaboration (PACS 18 [9]) was on the use of very large volumes at the physical pion mass. The calculation comprises only one lattice spacing and a single source-sink separation. Therefore, at the current stage, the study does not offer sufficient control over several systematic effects. The Mainz group (Mainz 18 [132]) has presented preliminary results for the axial charge, obtained by performing two-state fits to six different nucleon matrix elements (including the scalar and tensor charges), assuming that the mass gap to the excited state can be more reliably constrained in this way. Up to six source-sink separations per ensemble have been studied.

Two groups, PNDME and CalLat, have published results for $N_f = 2 + 1 + 1$, i.e., PNDME 16 [34], PNDME 18 [38], CalLat 17 [35] CalLat 18 [39]. While both groups share the staggered (HISQ) gauge ensembles generated by the MILC collaboration, they employ different discretizations in the valence quark sector: PNDME use O(a) improved Wilson fermions with the improvement coefficient $c_{\rm sw}$ set to its tadpole-improved tree-level value. By contrast, CalLat use the Möbius variant of domain wall fermions, which are fully O(a) improved. The CalLat set of ensembles includes three values of the lattice spacing, i.e., $a = 0.09$, 0.12,

and 0.15 fm, while PNDME added another set of ensembles at the finer lattice spacing of 0.06 fm to this collection. Both groups have included physical pion mass ensembles in their calculations. The operator matrix elements are renormalized nonperturbatively, using the Rome-Southampton method.

In order to control excited state contamination, PNDME perform multi-state fits, including up to four (three) energy levels in the two-point (three-point) correlation functions. By contrast, CalLat have employed the Feynman-Hellmann-inspired implementation of summed operator insertions described in Sec. 10.1.2. Plotting the summed correlator $S_A(\tau)$ as a function of the source-sink separation, they find that excited-state effects cannot be detected for $\tau \gtrsim 1.0$ fm at their level of statistics. After subtracting the leading contributions from excited states determined from two-state fits, they argue that the data for $S_A(\tau)$ can be described consistently down to $\tau \simeq 0.3$ fm.

We now proceed to discuss global averages for the axial charge, in accordance with the procedures in Sec. 10.2. For QCD with $N_f = 2+1+1$, the calculations of PNDME and CalLat pass all our quality criteria, and hence the latest results, i.e., PNDME 18 [38] and CalLat 18 [39] qualify for being included in a global average. Since both PNDME and CalLat use the gauge ensembles produced by MILC, we assume that the quoted statistical errors are 100% correlated, even though the range of pion masses and lattice spacings explored in Refs. [38] and [39] is not exactly identical. Since the two calculations differ by the valence quark action, and since systematic errors have been estimated independently, we restrict the correlations between PNDME 18 and CalLat 18 to the statistical error only. Performing a weighted average yields $g_A^{u-d} = 1.266(18)$ with $\chi^2/\text{dof} = 1.68$, where the error has been scaled by about 30% because of the large χ^2/dof. Given that the calculations of PNDME 18 and CalLat 18 are correlated, the large value of χ^2/dof indicates a tension between the two results. In this situation it is appropriate to adopt a more conservative approach: We estimate the axial charge to be represented by the interval $1.218 \le g_A^{u-d} \le 1.284$, where the lower bound is identified with the result of PNDME 18, while the upper bound is the weighted average plus the scaled 1σ uncertainty. Hence, for $N_f = 2+1+1$ we quote $g_A^{u-d} = 1.251(33)$ as the FLAG estimate, where the central value marks the mid-point of the interval, and half the width is taken to be the error.

For QCD with $N_f = 2+1$ dynamical quarks, the calculations of χQCD 18 [46] and Mainz 18 [132] are free of red tags. However, since the result from the latter is preliminary and published only as a proceedings article, it does not qualify for being included in a global average. Hence, for $N_f = 2+1$ we identify the FLAG average with the result quoted in χQCD 18 [46], i.e., $g_A^{u-d} = 1.254(16)(30)$.

In the two-flavour case, the results by the Mainz group [21, 24] qualify for an average, since other recent calculations employed only a single source-sink separation on most ensembles (RQCD 14 [22], QCDSF 13 [20]) or because only a single lattice spacing was used (ETM 15D [26], ETM 17B [28]). For $N_f = 2$ we quote the latest estimate g_A^{u-d} from Mainz 17 [24], adding statistical and systematic errors in quadrature and symmetrizing the error. To summarize, the FLAG averages for the axial charge read

$$N_f = 2+1+1: \quad g_A^{u-d} = 1.251(33) \quad \text{Refs. [38, 39]}, \tag{378}$$

$$N_f = 2+1: \quad g_A^{u-d} = 1.254(16)(30) \quad \text{Ref. [46]}, \tag{379}$$

$$N_f = 2: \quad g_A^{u-d} = 1.278(86) \quad \text{Ref. [24]} \tag{380}$$

Within errors, these averages are all compatible with the result of $g_A^{u-d} = 1.2724(23)$ quoted

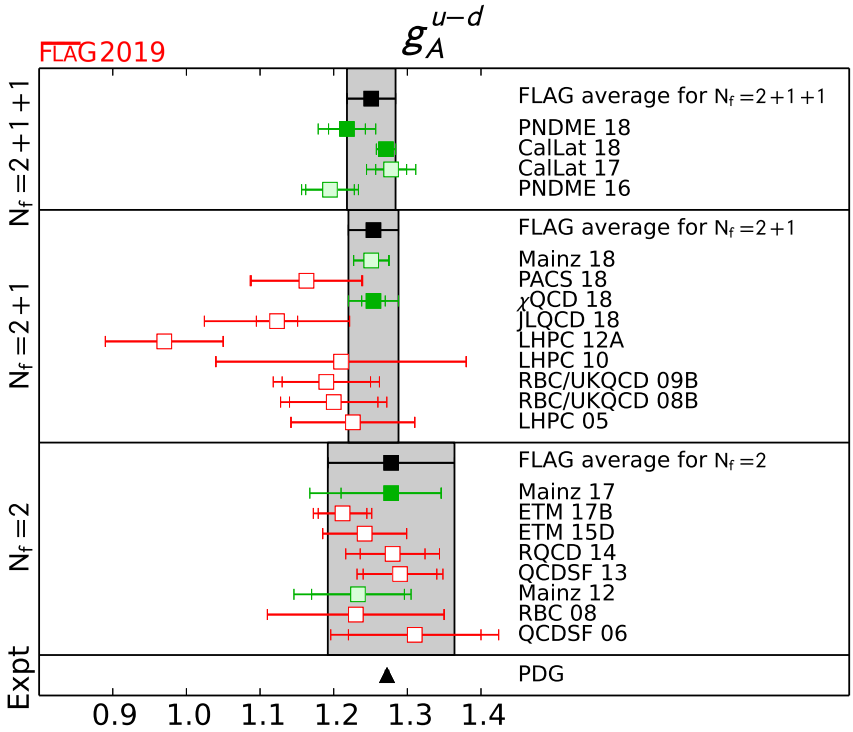

Figure 40: Lattice results and FLAG averages for the isovector axial charge g_A^{u-d} for $N_f = 2$, $2+1$, and $2+1+1$ flavour calculations.

by the PDG. While the most recent lattice calculations reproduce the axial charge at the level of a few percent or even better, the experimental result is more precise by an order of magnitude.

10.3.2 Results for g_S^{u-d}

Calculations of the isovector scalar charge have, in general, larger errors than the isovector axial charge as can be seen from the compilation given in Tab. 63 and plotted in Fig. 41. For comparison, Fig. 41 also shows a phenomenological result produced using the conserved vector current (CVC) relation [126].

Only a single calculation, PNDME 18 [38], which supersedes PNDME 16 [34] and PNDME 13 [31], meets all the criteria for inclusion in the average.

This 2+1+1 flavour mixed-action calculation was performed using the MILC HISQ ensembles, with a clover valence action. The 11 ensembles used include three pion mass values, $M_\pi \sim 135$, 225, 320 MeV, and four lattice spacings, $a \sim 0.06$, 0.09, 0.12, 0.15 fm. Note that four lattice spacings are required to meet the green star criteria, as this calculation is not fully $O(a)$ improved. Lattice size ranges between $3.3 \lesssim M_\pi L \lesssim 5.5$, and the set of ensembles includes three different volumes at a fixed pion mass $M_\pi \sim 225$ MeV and lattice spacing $a \sim 0.12$ fm. Physical point extrapolations were performed simultaneously, keeping only the leading order terms in the various expansion parameters. For the chiral extrapolation, these are the terms proportional to M_π^2, while the continuum extrapolation is performed using the term proportional to a, because the action and operators are not fully $O(a)$ improved. For the finite-volume extrapolation, the asymptotic limit of the χPT prediction, Eq. (375), is used.

Collaboration	Ref.	N_f	publication status	continuum extrapolation	chiral extrapolation	finite volume	renormalization	excited states	g_S^{u-d}
PNDME 18	[38]	2+1+1	A	★‡	★	★	★	★	1.022(80)(60)
PNDME 16	[34]	2+1+1	A	○‡	★	★	★	★	0.97(12)(6)
PNDME 13	[31]	2+1+1	A	■‡	■	★	★	★	0.72(32)
Mainz 18	[132]	2+1	C	★	○	★	★	★	1.22(11)
JLQCD 18	[49]	2+1	A	■	○	○	★	★	0.88(8)(3)(7)
LHPC 12	[137]	2+1	A	■‡	★	★	★	★	1.08(28)(16)
ETM 17	[30]	2	A	■	○	○	★	★	0.930(252)(48)(204)
RQCD 14	[22]	2	A	○	★	★	★	■	1.02(18)(30)

‡ The rating takes into account that the action is not fully O(a) improved by requiring an additional lattice spacing.

Table 63: Overview of results for g_S^{u-d}.

The Akaike Information Criterion is used to conclude that including more fit parameters is not justified based on the data.

Excited state contamination is controlled using two-state fits to between three and five source-sink time separations. Time separations range between $0.72 \lesssim \tau \lesssim 1.68$ fm, with all ensembles having at least two time separations greater than 1 fm. Renormalization was performed nonperturbatively using the RI-SMOM scheme and converted to $\overline{\text{MS}}$ at 2 GeV using 2-loop perturbation theory.

Regarding 2+1-flavour calculations, the Mainz 18 calculation meets all criteria for averaging, however as it is only a preliminary result published in proceedings it is not considered. The calculation was performed on the Wilson CLS ensembles, using four lattice spacings down to 0.05 fm and several pion masses down to ~ 200 GeV. Excited states were controlled using multi-state fits to several source-sink separations. The JLQCD 18 calculation, performed using overlap fermions on the Iwasaki gauge action, covered four pion masses down to 290 MeV. The lattice size was adjusted to keep $M_\pi L \geq 4$ in all four cases. However, the single lattice spacing of $a = 0.11$ fm does not meet the criteria for continuum extrapolation. The calculations presented in LHPC 12A used three different lattice actions, Wilson-clover, domain wall, and mixed action. Pion masses ranged down to near the physical pion mass. Data at two lattice spacings were produced with the domain wall and Wilson actions, however, the final result utilized only the single lattice spacing of $a = 0.116$ fm from the Wilson action. Because the action is not fully $O(a)$ improved, two lattice spacings are not sufficient for meeting the

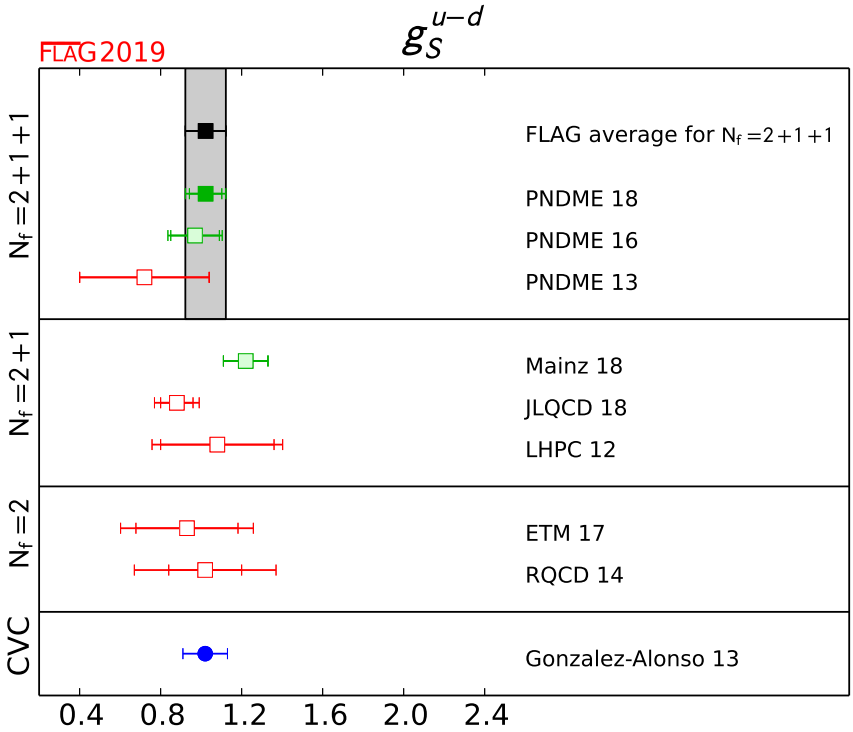

Figure 41: Lattice results and FLAG averages for the isovector scalar charge g_S^{u-d} for $N_f = 2$, $2+1$, and $2+1+1$ flavour calculations. Also shown is a phenomenological result obtained using the conserved vector current (CVC) relation [126] (circle).

quality criteria for the continuum extrapolation.

The two-flavour calculations in Tab. 63 include ETM 17, which employed twisted mass fermions on the Iwasaki gauge action[5]. This work utilized a single physical pion mass ensemble with lattice spacing $a \sim 0.09$ fm, and therefore does not meet the criteria for continuum extrapolation. The RQCD 14 calculation included three lattice spacings down to 0.06 fm and several pion masses down to near the physical point. While a study of excited state contamination was performed on some ensembles using multiple source-sink separations, many ensembles included only a single time separation, so it does not meet the criteria for excited states.

The final FLAG average for g_S^{u-d} is

$$N_f = 2+1+1: \qquad g_S^{u-d} = 1.022(80)(60) \qquad \text{Ref. [38].} \qquad (381)$$

10.3.3 Results for g_T^{u-d}

Estimates of the isovector tensor charge are currently the most precise of the isovector charges with values that are stable over time, as can be seen from the compilation given in Tab. 64 and plotted in Fig. 42. This is a consequence of the smaller statistical fluctuations in the raw data and the very mild dependence on a, M_π, and the lattice size $M_\pi L$. As a result, the

[5]The earlier work, ETM 15D [26], did not give a final value for g_S^{u-d} and is therefore not included in the tables.

Collaboration	Ref.	N_f	publication status	continuum extrapolation	chiral extrapolation	finite volume	renormalization	excited states	g_T^{u-d}
PNDME 18	[38]	2+1+1	A	★‡	★	★	★	★	0.989(32)(10)
PNDME 16	[34]	2+1+1	A	○‡	★	★	★	★	0.987(51)(20)
PNDME 15	[32, 33]	2+1+1	A	○‡	★	★	★	★	1.020(76)
PNDME 13	[31]	2+1+1	A	■‡	■	★	★	★	1.047(61)
Mainz 18	[132]	2+1	C	★	○	★	★	★	0.979(60)
JLQCD 18	[49]	2+1	A	■	○	○	★	★	1.08(3)(3)(9)
LHPC 12	[137]	2+1	A	■‡	★	★	★	★	1.038(11)(12)
RBC/UKQCD 10D	[42]	2+1	A	■	■	○	★	■	0.9(2)
ETM 17	[30]	2	A	■	○	○	★	★	1.004(21)(2)(19)
ETM 15D	[26]	2	A	■	○	○	★	★	1.027(62)
RQCD 14	[22]	2	A	○	★	★	★	■	1.005(17)(29)
RBC 08	[135]	2	A	■	■	■	★	■	0.93(6)

‡ The rating takes into account that the action is not fully O(a) improved by requiring an additional lattice spacing.

Table 64: Overview of results for g_T^{u-d}.

uncertainty due to the various extrapolations is small. Also shown for comparison in Fig. 42 are phenomenological results using measures of transversity [138–142].

Only the PNDME 18 [38] calculation, which supersedes PNDME 16 [34], PNDME 15 [32, 33] and PNDME 13 [31], meets all the criteria for inclusion in the average. The details for this calculation are the same as those for g_S^{u-d} described in the previous section (Sec. 10.3.2), except that three-state fits were used to remove excited-state effects.

For 2+1-flavour calculations, details for the Mainz 18, JLQCD 18, and LHPC 12A, calculations are identical to those presented previously in Sec. 10.3.2. The earlier RBC/UKQCD 10 calculation was performed using domain wall fermions on the Iwasaki gauge action, with two volumes and several pion masses. The lowest pion mass used was $M_\pi \sim 330$ MeV and does not meet the criteria for chiral extrapolation. In addition, the single lattice spacing and single source-sink separation do not meet the criteria for continuum extrapolation and excited states.

Two-flavour calculations include RQCD 14, with details identical to those described in Sec. 10.3.2. There are two calculations, ETM 15D and ETM 17, which employed twisted mass fermions on the Iwasaki gauge action. The earlier work utilized three ensembles, with three

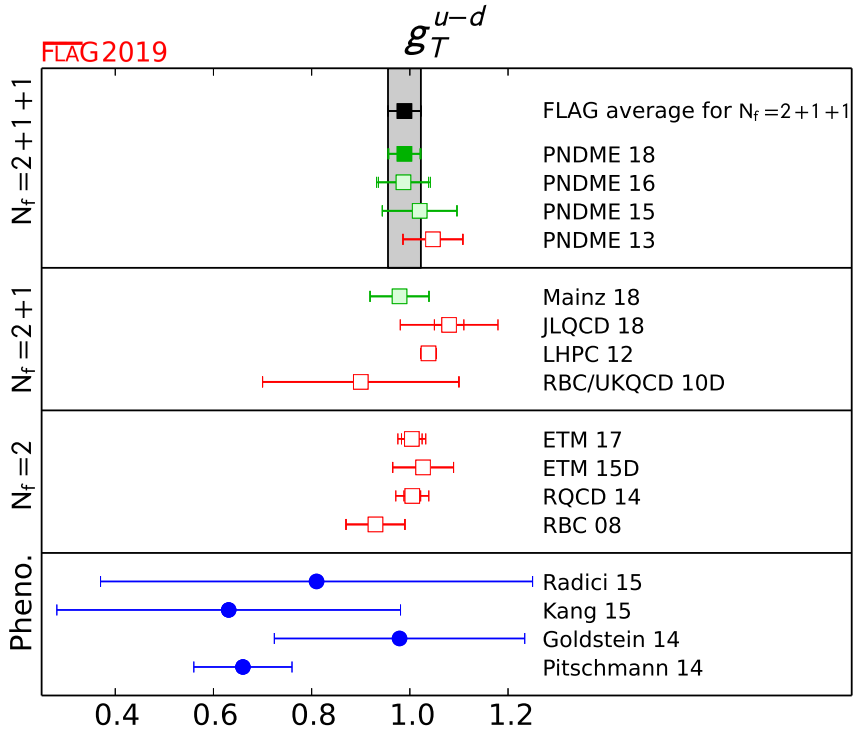

Figure 42: Lattice results and FLAG averages for the isovector tensor charge g_T^{u-d} for $N_f = 2$, $2+1$, and $2+1+1$ flavour calculations. Also shown are phenomenological results using measures of transversity [138–142] (circles).

volumes and two pion masses down to the physical point. The more recent work used only the physical pion mass ensemble. Both works used only a single lattice spacing $a \sim 0.09$ fm, and therefore do not meet the criteria for continuum extrapolation. The early work by RBC 08 with domain wall fermions used three heavy values for the pion mass, and a single value for the lattice spacing, volume, and source-sink separation, and therefore do not meet many of the criteria.

The final FLAG average for g_T^{u-d} is

$$N_f = 2+1+1: \qquad g_T^{u-d} = 0.989(32)(10) \qquad \text{Ref. [38].} \qquad (382)$$

10.4 Flavour Diagonal Charges

Three examples of interactions for which matrix elements of flavour-diagonal operators ($q\Gamma q$ where Γ defines the Lorentz structure of the bilinear quark operator) are needed are the neutral current interactions of neutrinos, elastic scattering of electrons off nuclei, and the scattering of dark matter off nuclei. In addition, these matrix elements also probe intrinsic properties of nucleons (the spin, the strangeness contribution and the electric dipole moment of the quarks) as explained below. For brevity, all operators are assumed to be appropriately renormalized as discussed in Sec. 10.1.3.

The matrix elements of the scalar operator, $\bar{q}q$ with flavour q, give the rate of change in the nucleon mass due to nonzero values of the corresponding quark mass. This relationship is

given by the Feynman-Hellmann theorem. The quantities of interest are the nucleon σ-term, $\sigma_{\pi N}$, and the strange and charm content of the nucleon, σ_s and σ_c,

$$\sigma_{\pi N} = m_{ud}\langle N|\overline{u}u + \overline{d}d|N\rangle\,, \tag{383}$$

$$\sigma_s = m_s\langle N|\overline{s}s|N\rangle\,, \tag{384}$$

$$\sigma_c = m_c\langle N|\overline{c}c|N\rangle\,. \tag{385}$$

Here m_{ud} is the average of the up and down quark masses and m_s (m_c) is the strange (charm) quark mass. The $\sigma_{\pi N,s,c}$ give the shift in M_N due to nonzero light-, strange- and charm-quark masses. The same matrix elements are also needed to quantify the spin independent interaction of dark matter with nucleons. Note that, while σ_b and σ_t are also phenomenologically interesting, they are unlikely to be calculated on the lattice. In principle, the heavy sigma terms can be estimated using $\sigma_{u,d,s}$ by exploiting the heavy-quark limit [143–145].

The matrix elements of the axial operator, $\overline{q}\gamma_\mu\gamma_5 q$, give the contribution, Δq, of quarks of flavour q to the spin of the nucleon:

$$\begin{aligned}\langle N|\overline{q}\gamma_\mu\gamma_5 q|N\rangle &= g_A^q\overline{u}_N\gamma_\mu\gamma_5 u_N,\\ g_A^q \equiv \Delta q &= \int_0^1 dx(\Delta q(x) + \Delta\overline{q}(x))\,.\end{aligned} \tag{386}$$

The charge g_A^q is thus the contribution of the spin of a quark of flavour q to the spin of the nucleon. It is also related to the first Mellin moment of the polarized parton distribution function (PDF), Δq, as shown in the second line in Eq. (384). Measurements by the European Muon collaboration in 1987 of the spin asymmetry in polarized deep inelastic scattering showed that the sum of the spins of the quarks contributes less than half of the total spin of the proton [146]. To understand this unexpected result, called the "proton spin crisis", it is common to start with Ji's sum rule [147] that provides a gauge invariant decomposition of the nucleon's total spin as

$$\frac{1}{2} = \sum_{q=u,d,s,c,\cdot}(\frac{1}{2}\Delta q + L_q) + J_g\,, \tag{387}$$

where $\Delta q/2 \equiv g_A^q/2$ is the contribution of the intrinsic spin of a quark with flavour q; L_q is the orbital angular momentum of that quark; and J_g is the total angular momentum of the gluons. Thus, to obtain the spin of the proton starting from QCD, requires calculating the contributions of the three terms: the spin and orbital angular momentum of the quarks, and the angular momentum of the gluons. Lattice-QCD calculations of the various matrix elements needed to extract the three contributions are underway. An alternate decomposition of the spin of the proton has been provided by Jaffe and Manohar [148]. The two formulations differ in the decomposition of the contributions of the quark orbital angular momentum and of the gluons. The contribution of the quark spin, which is the subject of this review and given in Eq. (384), is the same in both formulations.

The tensor charges are defined as the matrix elements of the tensor operator, $\overline{q}\sigma^{\mu\nu}q$ with $\sigma^{\mu\nu} = \{\gamma_\mu, \gamma_\nu\}/2$:

$$g_T^q\overline{u}_N\sigma_{\mu\nu}u_N = \langle N|\overline{q}\sigma_{\mu\nu}q|N\rangle\,, \tag{388}$$

These flavour-diagonal tensor charges $g_T^{u,d,s,c}$ quantify the contributions of the u, d, s, c quark electric dipole moments (EDM) to the neutron electric dipole moment (nEDM) [32, 149].

Since particles can have an EDM only due to P and T (or CP assuming CPT is a good symmetry) violating interactions, the nEDM is a very sensitive probe of new sources of CP violation that arise in most extensions of the SM designed to explain nature at the TeV scale. The current experimental bound on the nEDM is $d_n < 2.9\times10^{-26}$ e cm [150], while the known CP violation in the SM implies $d_n < 10^{-31}$ e cm [151]. A nonzero result over the intervening five orders of magnitude would signal new physics. Planned experiments aim to reduce the bound to around 10^{-28} e cm. A discovery or reduction in the bound from these experiments will put stringent constraints on many BSM theories, provided the matrix elements of novel CP-violating interactions, of which the quark EDM is one, are calculated with the required precision.

One can also extract these tensor charges from the zeroth moment of the transversity distributions that are measured in many experiments including Drell-Yan and semi-inclusive deep inelastic scattering (SIDIS). Of particular importance is the active program at Jefferson Lab (JLab) to measure them [128, 129]. Transversity distributions describe the net transverse polarization of quarks in a transversely polarized nucleon. Their extraction from the data taken over a limited range of Q^2 and Bjorken x is, however, not straightforward and requires additional phenomenological modeling. At present, lattice-QCD estimates of $g_T^{u,d,s}$ are the most accurate [32, 130, 131] as can be deduced from Fig. 42. Future experiments will significantly improve the extraction of the transversity distributions. Thus, accurate calculations of the tensor charges using lattice QCD will continue to help elucidate the structure of the nucleon in terms of quarks and gluons and provide a benchmark against which phenomenological estimates utilizing measurements at JLab and other experimental facilities worldwide can be compared.

The methodology for the calculation of flavour-diagonal charges is also well-established. The major challenges are the much larger statistical errors in the disconnected contributions for the same computational cost and the need for the additional calculations of the isosinglet renormalization factors.

10.4.1 Results for $g_A^{u,d,s}$

A compilation of recent results for the flavour-diagonal axial charges for the proton is given in Tab. 65 and plotted in Fig. 43. Results for the neutron can be obtained by interchanging the u and d flavor indices. Only two calculations qualify for global averages, the PNDME 18A for 2+1+1 flavours [37] and the χQCD 18 for 2+1 flavours [46]. The global averages given below are, therefore, the same as the corresponding results given in Tab. 65.

The 2+1+1 flavour FLAG results for the axial charges $g_A^{u,d,s}$ of the proton are

$$N_f = 2+1+1: \qquad g_A^u = \quad 0.777(25)(30) \qquad \text{Ref. [37]}, \tag{389}$$

$$N_f = 2+1+1: \qquad g_A^d = -0.438(18)(30) \qquad \text{Ref. [37]}, \tag{390}$$

$$N_f = 2+1+1: \qquad g_A^s = -0.053(8) \qquad \text{Ref. [37]}. \tag{391}$$

These PNDME 18A [37] results were obtained using the 2+1+1 flavour clover-on-HISQ formulation. The connected contributions were obtained on 11 HISQ ensembles generated by the MILC collaboration with $a \approx 0.057$, 0.87, 0.12 and 0.15 fm, $M_\pi \approx 135$, 220 and 320 MeV, and $3.3 < M_\pi L < 5.5$. The light disconnected contributions were obtained on six of these

Collaboration	Ref.	N_f	publication status	continuum extrapolation	chiral extrapolation	finite volume	renormalization	excited states	Δu	Δd
PNDME 18A	[37]	2+1+1	A	★‡	★	★	★	★	0.777(25)(30)#	−0.438(18)(30)#
χQCD 18	[46]	2+1	A	○	★	★	★	★	0.847(18)(32)$	−0.407(16)(18)$
ETM 17C	[29]	2	A	■	○	○	★	★	0.830(26)(4)	−0.386(16)(6)
									Δs	
PNDME 18A	[37]	2+1+1	A	★‡	★	★	★	★	−0.053(8)#	
χQCD 18	[46]	2+1	A	○	★	★	★	★	−0.035(6)(7)$	
JLQCD 18	[49]	2+1	A	■	○	○	★	★	−0.046(26)(9)#	
χQCD 15	[45]	2+1	A	■	○	■	★	★	−0.0403(44)(78)#	
Engelhardt 12	[152]	2+1	A	■	○	■	★	★	−0.031(17)#	
ETM 17C	[29]	2	A	■	○	○	★	★	−0.042(10)(2)	

Assumed that $Z_A^{n.s.} = Z_A^s$.

‡ The rating takes into account that the action is not fully O(a) improved by requiring an additional lattice spacing.

$ For this partially quenched analysis the criteria are applied to the unitary points.

Table 65: Overview of results for g_A^q.

ensembles with the lowest pion mass $M_\pi \approx 220$ MeV, while the strange disconnected contributions were obtained on seven ensembles, i.e., including an additional one at $a \approx 0.087$ fm and $M_\pi \approx 135$ MeV. The excited state and the chiral-continuum fits were done separately for the connected and disconnected contributions, which introduces a systematic that is hypothesied to be small as explained in Ref. [37]. The analysis of the excited-state contamination, discussed in Sec. 10.1.2, was done using three-state fits for the connected contribution and two-state fits for the disconnected contributions. The chiral-continuum extrapolation was done keeping the leading correction terms proportional to M_π^2 and a in both cases, and the leading finite-volume correction in $M_\pi L$ was included in the analysis of the connected contributions. The isovector renormalization factor, used for all three flavour diagonal operators, was calculated on the lattice in the RI-SMOM scheme and converted to $\overline{\text{MS}}$. The difference

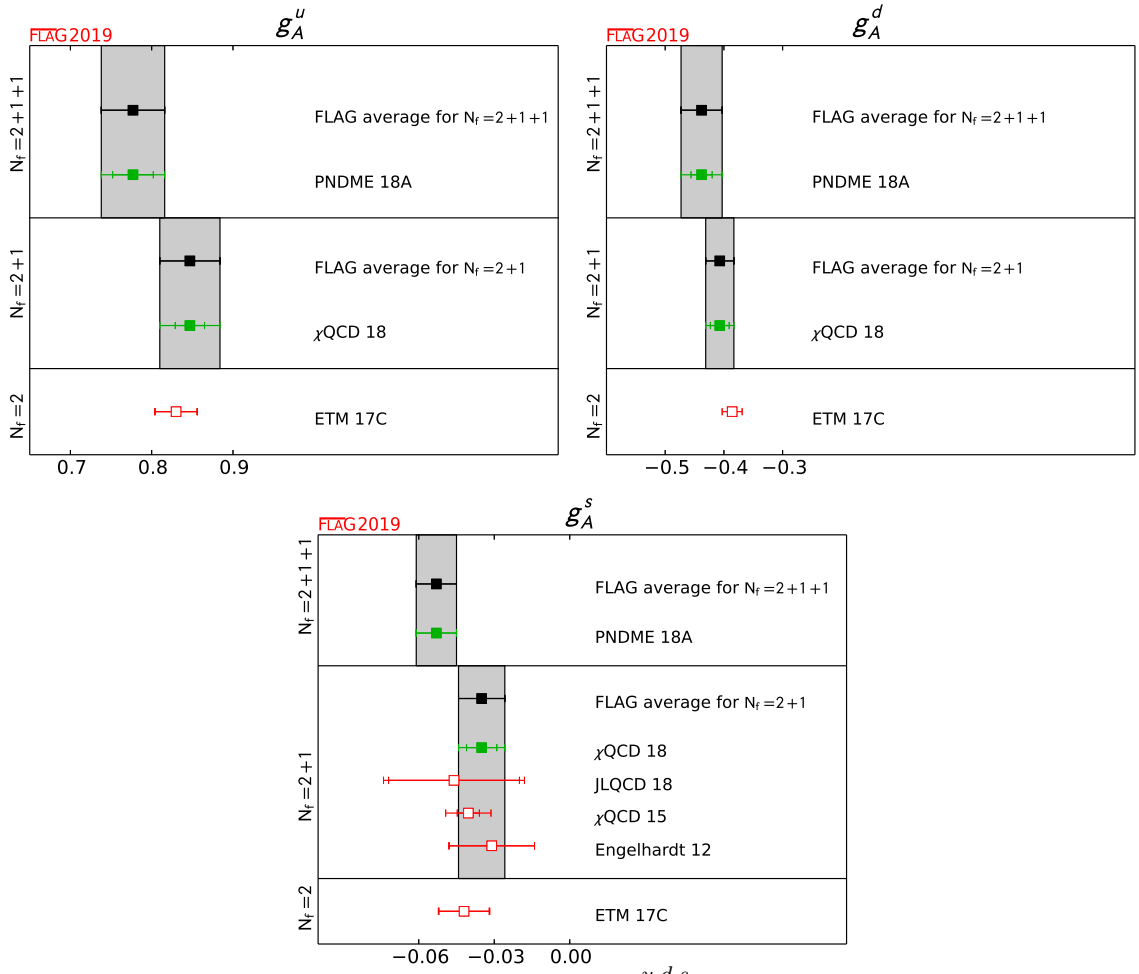

Figure 43: Lattice results and FLAG averages for $g_A^{u,d,s}$ for the $N_f = 2$, $2+1$, and $2+1+1$ flavour calculations.

due to flavor mixing for the singlet case is small as discussed in Sec. 10.1.3.

The 2+1 flavour FLAG results from χQCD 18 were obtained using the overlap-on-domain-wall formalism [46]. Three domain-wall ensembles with lattice spacings 0.143, 0.11 and 0.083 fm and sea-quark pion masses M_π = 171, 337 and 302 MeV, respectively, were analyzed. In addition to the three approximately unitary points, the paper presents data for an additional 4–5 valence quark masses on each ensemble, i.e., partially quenched data. Separate excited-state fits were done for the connected and disconnected contributions. The continuum, chiral and volume extrapolation to the combined unitary and nonunitary data is made including terms proportional to both $M^2_{\pi,\text{valence}}$ and $M^2_{\pi,\text{sea}}$, and two $O(a^2)$ discretization terms for the two different domain wall actions. With just three unitary points, not all the coefficients are well constrained. The $M_{\pi,sea}$ dependence is omitted and considered as a systematic, and a prior is used for the coefficients of the a^2 terms to stabilize the fit. These χQCD 18 2+1 flavour results for the proton, which supersede the χQCD 15 [45] analysis, are

$$N_f = 2+1: \qquad g_A^u = \quad 0.847(18)(32) \qquad \text{Ref. [46]}, \tag{392}$$

$$N_f = 2+1: \qquad g_A^d = -0.407(16)(18) \qquad \text{Ref. [46]}, \tag{393}$$

$$N_f = 2+1: \qquad g_A^s = -0.035(6)(7) \qquad \text{Ref. [46].} \tag{394}$$

The JLQCD 18 [49], ETM 17C [29] and Engelhardt 12 [152] calculations were not considered for the averages as they did not satisfy the criteria for the continuum extrapolation. All three calculations were done at a single lattice spacing. The JLQCD 18 calculation used overlap fermions and the Iwasaki gauge action. They perform a chiral fit using data at four pion masses in the range 290–540 MeV. Finite volume corrections are assumed to be negligible since each of the two pairs of points on different lattice volumes satisfy $M_\pi L \geq 4$. The ETM 17C calculation is based on a single twisted mass ensemble with $M_\pi = 130$ MeV, $a = 0.094$ and a relatively small $M_\pi L = 2.98$. Engelhardt 12 calculation was done on three asqtad ensembles with $M_\pi = 293$, 356 and 495 MeV, but all at a single lattice spacing $a = 0.124$ fm.

Results for g_A^s were also presented recently by LHPC in Ref. [5]. However, this calculation is not reviewed as it has been performed on a single ensemble with $a = 0.114$ and a heavy pion mass value of $M_\pi \approx 317$ MeV.

10.4.2 Results for $g_S^{u,d,s}$ from direct and hybrid calculations of the matrix elements

The sigma terms $\sigma_q = m_q\langle N|\bar{q}q|N\rangle = m_q g_S^q$ or the quark mass fractions $f_{T_q} = \sigma_q/M_N$ are normally computed rather than g_S^q. These combinations have the advantage of being renormalization group invariant in the continuum, and this holds on the lattice for actions with good chiral properties, see Sec. 10.1.3 for a discussion. In order to aid comparison with phenomenological estimates, e.g., from π–N scattering [153–155], the light quark sigma terms are usually added to give the πN sigma term, $\sigma_{\pi N} = \sigma_u + \sigma_d$. The direct evaluation of the sigma terms involves the calculation of the corresponding three-point correlation functions for different source-sink separations τ. For $\sigma_{\pi N}$ there are both connected and disconnected contributions, while for most lattice fermion formulations only disconnected contributions are needed for σ_s. The techniques typically employed lead to the availability of a wider range of τ for the disconnected contributions compared to the connected ones (both, however, suffer from signal to noise problems for large τ, as discussed in Sec. 10.1) and we only comment on the range of τ computed for the latter in the following.

Recent results for $\sigma_{\pi N}$ and for σ_s from the direct approach are compiled in Tab. 66. For both quantities, only the results from χQCD 15A [44] qualify for global averaging. In this mixed action study, three RBC/UKQCD $N_f = 2+1$ domain wall ensembles are analysed comprising two lattice spacings, $a = 0.08$ fm with $M_{\pi,\text{sea}} = 300$ MeV and $a = 0.11$ fm with $M_{\pi,\text{sea}} = 330$ MeV and 139 MeV. Overlap fermions are employed with a number of nonunitary valence quark masses. The connected three-point functions are measured with three values of τ in the range 0.9–1.4 fm. A combined chiral, continuum and volume extrapolation is performed for all data with $M_\pi < 350$ MeV. The leading order expressions are taken for the lattice-spacing and volume dependence while partially quenched $SU(2)$ HBχPT up to M_π^3 terms models the chiral behaviour for $\sigma_{\pi N}$. The strange quark sigma term has a milder dependence on the pion mass and only the leading order quadratic terms are included in this case.

The lack of other qualifying studies is an indication of the difficulty and computational expense of performing these calculations. Nonetheless, this situation is likely to improve in the future. We note that although the recent analyses, ETM 16A [27] and JLQCD 18 [49], are both performed at a single lattice spacing ($a = 0.09$ fm and 0.11 fm, respectively), they

Collaboration	Ref.	N_f	publication status	continuum extrapolation	chiral extrapolation	finite volume	renormalization	excited states	$\sigma_{\pi N}$ [MeV]	σ_s [MeV]
JLQCD 18	[49]	2+1	A	■	○	○	na/na	★	26(3)(5)(2)	17(18)(9)
χQCD 15A	[44]	2+1	A	○	★	★	na/na	★	45.9(7.4)(2.8)[$]	40.2(11.7)(3.5)[$]
χQCD 13A	[43]	2+1	A	■	■	○	−/na	★	−	33.3(6.2)[$]
JLQCD 12A	[48]	2+1	A	■	○	○	−/na	★	−	0.009(15)(16)$\times m_N$[†]
Engelhardt 12	[152]	2+1	A	■	○	■	−/na	★	−	0.046(11)$\times m_N$[†]
ETM 16A	[27]	2	A	■	○	○	na/na	★	37.2(2.6)$(^{4.7}_{2.9})$	41.1(8.2)$(^{7.8}_{5.8})$
RQCD 16	[23]	2	A	○	★	★	na/★	■	35(6)	35(12)
MILC 12C	[156]	2+1+1	A	★	★	★	−/○	★	−	0.44(8)(5)$\times m_s$[¶§]
MILC 12C	[156]	2+1	A	★	○	★	−/○	★	−	0.637(55)(74)$\times m_s$[¶§]
MILC 09D	[157]	2+1	A	★	○	★	−/na	★	−	59(6)(8)[§]

The renormalization criteria is given for $\sigma_{\pi N}$ (first) and σ_s (second). The label na indicates that no renormalization is required.

[$] For this partially quenched analysis the criteria are applied to the unitary points.
† This study computes the strange quark fraction f_{T_s}/m_N.
§ This study employs a hybrid method, see Ref. [157].
¶ The matrix element $\langle N|\bar{s}s|N\rangle$ at the scale $\mu = 2$ GeV in the $\overline{\text{MS}}$ scheme is computed.

Table 66: Overview of results for $\sigma_{\pi N}$ and σ_s from the direct approach (above) and σ_s from the hybrid approach (below).

satisfy the criteria for chiral extrapolation, finite volume and excited states. ETM 16A is a single ensemble study with $N_f = 2$ twisted mass fermions with a pion mass close to the physical point and $M_\pi L = 3.0$. Excited states are investigated utilizing $\tau = 0.9$ fm up to $\tau = 1.7$ fm for the connected three-point functions. JLQCD utilize $N_f = 2+1$ overlap fermion ensembles with pion masses reaching down to 293 MeV ($M_\pi L = 4.0$) and apply techniques which give a wide range of τ for the connected contribution, with the final results extracted from $\tau \geq 1.2$ fm.

RQCD in RQCD 16 [23] investigate the continuum, physical quark mass and infinite-volume limits, where the lattice spacing spans the range 0.06–0.08 fm, the minimum M_π is 150 MeV and $M_\pi L$ is varied between 3.4 to 6.7 at $M_\pi = 290$ MeV. This $N_f = 2$ study has a red tag for the excited state criterion as multiple source-sink separations for the connected three-point functions are only computed on a subset of the ensembles. Clover fermions are

employed and the lack of good chiral properties for this action means that there is mixing between quark flavours under renormalization when determining σ_s and a gluonic term needs to be considered for full $O(a)$ improvement (which has not been included, see Sec. 10.1.3 for a discussion).

Earlier work focuses only on σ_s. The analysis of JLQCD 12A [48], is performed on the same set of ensembles as the JLQCD 18 study discussed above and in addition includes smaller volumes for the lightest two pion masses.[6] No significant finite-volume effects are observed. Engelhardt 12 [152] and χQCD 13A [43] have less control over the systematics. The former is a single lattice spacing analysis restricted to small spatial volumes while the latter is a partially quenched study on a single ensemble with unitary $M_\pi > 300$ MeV.

MILC have also computed σ_s using a hybrid method [157] which makes use of the Feynman-Hellmann (FH) theorem and involves evaluating the matrix element $\langle N|\int d^4x\,\bar{s}s|N\rangle$.[7] This method is applied in MILC 09D [157] to the $N_f = 2+1$ Asqtad ensembles with lattice spacings $a = 0.06, 0.09, 0.12$ fm and values of M_π ranging down to 224 MeV. A continuum and chiral extrapolation is performed including terms linear in the light-quark mass and quadratic in a. As the coefficient of the discretisation term is poorly determined, a Bayesian prior is used, with a width corresponding to a 10% discretisation effect between the continuum limit and the coarsest lattice spacing.[8] A similar updated analysis is presented in MILC 12C [156], with an improved evaluation of $\langle N|\int d^4x\,\bar{s}s|N\rangle$ on a subset of the $N_f = 2+1$ Asqtad ensembles. The study is also extended to HISQ $N_f = 2+1+1$ ensembles comprising four lattice spacings with $a = 0.06 - 0.15$ fm and a minimum pion mass of 131 MeV. Results are presented for $g_S^s = \langle N|\bar{s}s|N\rangle$ (in the $\overline{\text{MS}}$ scheme at 2 GeV) rather than for σ_s. The scalar matrix element is renormalized for both three and four flavours using the 2-loop factor for the Asqtad action [159]. The error incurred by applying the same factor to the HISQ results is expected to be small.[9]

Both MILC 09D and MILC 12C achieve green tags for all the criteria, see Tab. 66. As the same set of Asqtad ensembles is utilized in both studies we take MILC 12C as superseding MILC 09D for the three flavour case. The global averaging is discussed in Sec. 10.4.4.

10.4.3 Results for $g_S^{u,d,s}$ using the Feynman-Hellmann theorem

An alternative approach for accessing the sigma terms is to determine the slope of the nucleon mass as a function of the quark masses, or equivalently, the squared pseudoscalar meson masses. The Feynman-Hellman (FH) theorem gives

$$\sigma_{\pi N} = m_u \frac{\partial M_N}{\partial m_u} + m_d \frac{\partial M_N}{\partial m_d} \approx M_\pi^2 \frac{\partial M_N}{\partial M_\pi^2}, \qquad \sigma_s = m_s \frac{\partial M_N}{\partial m_s} \approx \frac{1}{2} M_{\bar{s}s}^2 \frac{\partial M_N}{\partial M_{\bar{s}s}^2}, \tag{395}$$

where the fictitious $\bar{s}s$ meson has a mass squared $M_{\bar{s}s}^2 = 2M_K^2 - M_\pi^2$. In principle this is a straightforward method as the nucleon mass can be extracted from fits to two-point correlation functions, and a further fit to M_N as a function of M_π (and also M_K for σ_s) provides the slope. Nonetheless, this approach presents its own challenges: a functional form for the

[6] JLQCD also determine f_{T_s} in Ref. [158] in a single lattice spacing study on small volumes with heavy pion masses.

[7] Note that in the direct method the matrix element $\langle N|\int d^3x\,\bar{s}s|N\rangle$, involving the spatial volume sum, is evaluated for a fixed timeslice.

[8] This is consistent with discretisation effects observed in other quantities at $a = 0.12$ fm.

[9] At least at 1-loop the Z factors for HISQ and Asqtad are very similar, cf. Ref. [160].

Collaboration	Ref.	N_f	publication status	continuum extrapolation	chiral extrapolation	finite volume	$\sigma_{\pi N}$ [MeV]	σ_s [MeV]
ETM 14A	[161]	2+1+1	A	★	○	○	64.9(1.5)(13.2)$^{\triangle}$	–
BMW 15	[162]	2+1	A	★‡	★	★	38(3)(3)	105(41)(37)
Junnarkar 13	[163]	2+1	A	○	○	○	–	48(10)(15)
Shanahan 12	[164]	2+1	A	■	○	○	45(6)/51(7)*	21(6)/59(6)*
JLQCD 12A	[48]	2+1	A	■	○	○	–	0.023(29)(28)$\times m_N{}^{\dagger}$
QCDSF 11	[165]	2+1	A	■	■	○	31(3)(4)	71(34)(59)
BMW 11A	[166]	2+1	A	○‡	★	○	39(4)($^{18}_{7}$)	67(27)($^{55}_{47}$)
Martin Camalich 10	[167]	2+1	A	■	★	■	59(2)(17)	−4(23)(25)
PACS-CS 09	[25]	2+1	A	■	★	■	75(15)	–
QCDSF 12	[19]	2	A	○	★	○	37(8)(6)	–
JLQCD 08B	[47]	2	A	■	○	■	53(2)($^{+21}_{-7}$)	–

$^{\triangle}$ Two results for $\sigma_{\pi N}$ are quoted arising from different fit ansätze to the nucleon mass. The systematic error is the same as in Ref. [168] for a combined $N_f = 2$ and $N_f = 2 + 1 + 1$ analysis [169].

‡ The rating takes into account that the action is not fully O(a) improved by requiring an additional lattice spacing.

* Two results are quoted.

† This study computes the strange quark fraction $f_{T_s} = \sigma_s/m_N$.

Table 67: Overview of results for $\sigma_{\pi N}$ and σ_s from the Feynman-Hellmann approach.

chiral behaviour of the nucleon mass is needed, and while baryonic χPT (BχPT) is the natural choice, the convergence properties of the different formulations are not well established. Results are sensitive to the formulation chosen and the order of the expansion employed. If there is an insufficient number of data points when implementing higher order terms, the coefficients are sometimes fixed using additional input, e.g., from analyses of experimental data. This may influence the slope extracted. Simulations with pion masses close to or bracketing the physical point can alleviate these difficulties. In some studies the nucleon mass is used to set the lattice spacing. This naturally forces the fit to reproduce the physical nucleon mass at the physical point and may affect the extracted slope.

An overview of recent determinations of $\sigma_{\pi N}$ and σ_s is given in Tab. 67. Note that the renormalization and excited state criteria are not applied.[10] We do not impose the latter

[10]Renormalization is normally not required in the Feynman-Hellmann approach when computing the sigma terms. However, when employing clover fermions one must take care of the mixing between quark flavours when renormalizing the quark masses that appear in Eq. (393).

since a wide range of source-sink separations are available for nucleon two-point functions and ground state dominance is normally achieved.

There are several results for $\sigma_{\pi N}$ that can be included in a global average. For $N_f = 2$, one study meets the selection criteria.[11] The analysis of QCDSF 12 [19] employs nonperturbatively improved clover fermions over three lattice spacings ($a = 0.06 - 0.08$ fm) with pion masses reaching down to around 160 MeV. Finite volume corrected nucleon masses are extrapolated via $O(p^4)$ covariant BχPT with three free parameters. The other coefficients are taken from experiment, phenomenology or FLAG, with the corresponding uncertainties accounted for in the fit for those coefficients that are not well known. The nucleon mass is used to set the scale. A novel feature of this study is that a direct determination of $\sigma_{\pi N}$ at around $M_\pi = 290$ MeV was used as an additional constraint on the slope.

Turning to $N_f = 2+1$, two studies performed by the BMW collaboration are relevant. In BMW 11A [166], stout smeared tree-level clover fermions are employed on 15 ensembles with simulation parameters encompassing $a = 0.06$–0.12 fm, $M_\pi \sim 190$–550 MeV and $M_\pi L \gtrsim 4$. Taylor, Padé and covariant $SU(3)$ BχPT fit forms are considered. Due to the use of smeared gauge links, discretisation effects are found to be mild even though the fermion action is not fully $O(a)$ improved. Fits are performed including an $O(a)$ or $O(a^2)$ term and also without a lattice-spacing dependent term. Finite volume effects were assessed to be small in an earlier work [171]. The final results are computed considering all combinations of the fit ansatz weighted by the quality of the fit. In BMW 15 [162], a more extensive analysis on 47 ensembles is presented for HEX-smeared clover fermions involving five lattice spacings and pion masses reaching down to 120 MeV. Bracketing the physical point reduces the reliance on a chiral extrapolation. Joint continuum, chiral and infinite-volume extrapolations are carried out for a number of fit parameterisations with the final results determined via the Akaike information criterion procedure [115]. Although only $\sigma_{\pi N}$ is accessible in the FH approach in the isospin limit, the individual quark fractions $f_{T_q} = \sigma_q/M_N$ for $q = u, d$ for the proton and the neutron are also quoted in BMW 15, using isospin relations.[12]

Regarding $N_f = 2+1+1$, there is only one recent study. In ETM 14A [161], fits are performed to the nucleon mass utilizing $SU(2)$ χPT for data with $M_\pi \geq 213$ MeV as part of an analysis to set the lattice spacing. The expansion is considered to $O(p^3)$ and $O(p^4)$, with two and three of the coefficients as free parameters, respectively. The difference between the two fits is taken as the systematic error. No discernable discretisation or finite-volume effects are observed where the lattice spacing is varied over the range $a = 0.06$–0.09 fm and the spatial volumes cover $M_\pi L = 3.4$ up to $M_\pi L > 5$. The results are unchanged when a near physical point $N_f = 2$ ensemble is added to the analysis in Ref. [168].

Other determinations of $\sigma_{\pi N}$ in Tab. 67 receive one or more red tags. JLQCD 08B [47], PACS-CS 09 [25] and QCDSF 11 [165] are single lattice spacing studies. In addition, the volume for the minimum pion mass is rather small for JLQCD 08B and PACS-CS 09, while QCDSF 11 is restricted to heavier pion masses.

We also consider publications that are based on results for baryon masses found in the literature. As different lattice setups (in terms of N_f, lattice actions, etc.) will lead to different systematics, we only include works in Tab. 67 which utilize a single setup. These correspond to Shanahan 12 [164] and Martin Camalich 10 [167], which fit PACS-CS data [173] (the

[11] ETMC also determine $\sigma_{\pi N}$ in Ref. [170] as part of an $N_f = 2$ analysis to determine the lattice spacing from the nucleon mass. However, no final result is given.

[12] These isospin relations were also derived in Ref. [172].

PACS-CS 09 study is also based on these results). Note that Shanahan 12 avoids a red tag for the volume criterion as the lightest pion mass ensemble is omitted. Recent studies which combine data from different setups/collaborations are displayed for comparison in Figs. 44 and 45 in the next section.

Several of the above studies have also determined the strange quark sigma term. This quantity is difficult to access via the Feynman-Hellmann method since in most simulations the physical point is approached by varying the light-quark mass, keeping m_s approximately constant. While additional ensembles can be generated, it is hard to resolve a small slope with respect to m_s. Such problems are illustrated by the large uncertainties in the results from BMW 11A and BMW 15. Alternative approaches have been pursued in QCDSF 11, where the physical point is approached along a trajectory keeping the average of the light- and strange-quark masses fixed, and JLQCD 12A [48], where quark mass reweighting is applied. The latter is a single lattice spacing study. One can also fit to the whole baryon octet and apply $SU(3)$ flavour symmetry constraints as investigated in, e.g., Martin Camalich 10, Shanahan 12, QCDSF 11 and BMW 11A.

The determinations of σ_s in BMW 11A and BMW 15 qualify for averaging. The mixed action study of Junnarkar 13 [163] with domain wall valence fermions on MILC $N_f = 2+1$ Asqtad ensembles also passes the FLAG criteria. The derivative $\partial M_N/\partial m_s$ is determined from simulations above and below the physical strange quark mass for M_π around 240–675 MeV. The resulting values of σ_s are extrapolated quadratically in M_π. The quark fraction $f_{T_s} = \sigma_s/M_N$ exhibits a milder pion-mass dependence and extrapolations of this quantity were also performed using ansätze linear and quadratic in M_π. A weighted average of all three fits was used to form the final result. Two lattice spacings were analysed, with a around 0.09 fm and 0.12 fm, however, discretisation effects could not be resolved. The global averaging of all calculations that qualify is discussed in the next section.

10.4.4 Summary of Results for $g_S^{u,d,s}$

We consider computing global averages of results determined via the direct, hybrid and Feynman-Hellmann (FH) methods. Beginning with $\sigma_{\pi N}$, Tabs. 66 and 67 show that for $N_f = 2+1+1$ only ETM 14A (FH) satisfies the selection criteria. We take this result as our average for the four flavour case.

$$N_f = 2+1+1: \qquad \sigma_{\pi N} = 64.9(1.5)(13.2)\ \text{MeV} \qquad \text{Ref. [161].} \tag{396}$$

For $N_f = 2+1$ we form an average from the BMW 11A (FH), BMW 15 (FH) and χQCD 15A (direct) results, yielding

$$N_f = 2+1: \qquad \sigma_{\pi N} = 39.7(3.6)\ \text{MeV} \qquad \text{Refs. [44, 162, 166].} \tag{397}$$

Note that both BMW results are included as they were obtained on independent sets of ensembles (employing different fermion actions). The average is dominated by the BMW 15 calculation, which has much smaller overall errors compared to the other two studies.

Turning to the results for $N_f = 2$, only QCDSF 12 (FH) qualifies. This result forms our average

$$N_f = 2: \qquad \sigma_{\pi N} = 37(8)(6)\ \text{MeV} \qquad \text{Ref. [19].} \tag{398}$$

Considering σ_s and the calculations detailed in Tab. 66, there is again only a single 2+1+1 flavour study, MILC 12C (hybrid), which satisfies the quality criteria. In order to convert the result for $\langle N|\bar{s}s|N\rangle$ given in this work to a value for σ_s, we multiply by the appropriate FLAG average for m_s given in Eq. (35). This gives our average for four flavours.

$$N_f = 2+1+1: \qquad \sigma_s = 41.0(8.8)\ \text{MeV} \qquad \text{Ref. [156].} \tag{399}$$

For $N_f = 2+1$ we perform a weighted average of BMW 11A (FH), MILC 12C (hybrid), Junnarkar 13 (FH), BMW 15 (FH) and χQCD 15A (direct). MILC 09D [157] also passes the FLAG selection rules, however, this calculation is superseded by MILC 12C. As for Eq. (397), the strangeness scalar matrix element determined in the latter study is multiplied by the three flavour FLAG average for m_s given in Eq. (33). There are correlations between the MILC 12C and Junnarkar 13 results as there is some overlap between the sets of Asqtad ensembles used in both cases. To be conservative we take the statistical errors for these two studies to be 100% correlated. The global average is

$$N_f = 2+1: \qquad \sigma_s = 52.9(7.0)\ \text{MeV} \qquad \text{Refs. [44, 156, 162, 163, 166].} \tag{400}$$

Given that all of the $N_f = 2$ studies have at least one red tag we are not able to give an average in this case.

All the results for $\sigma_{\pi N}$ and σ_s are displayed in Figs. 44 and 45 along with the averages given above. Note that where f_{T_s} is quoted in Tabs. 66 and 67, we multiply by the experimental proton mass in order to include the results in the figures. Those results which pass the FLAG criteria, shown in green, are consistent within one standard deviation with the averages for each N_f, and considering the size of the uncertainties in the averages no significant N_f-dependence is observed. However, there is some fluctuation in the central values, in particular, when taking the lattice results as a whole into account, and we caution the reader that the averages may change as new results become available.

Also shown for comparison in the figures are determinations from the FH method which utilize more than one lattice data set [168, 174–182] as well as results for $\sigma_{\pi N}$ obtained from recent analyses of π-N scattering [153–155, 183]. There is some tension, at the level of three to four standard deviations, between the lattice average for $N_f = 2+1$ and Hoferichter et al. [155], who quote a precision similar to that of the average.

Finally we remark that, by exploiting the heavy-quark limit, the light- and strange-quark sigma terms can be used to estimate σ_q for the charm, bottom and top quarks [143–145]. The resulting estimate for the charm quark, see, e.g., the RQCD 16 $N_f = 2$ analysis of Ref. [23] that reports $f_{T_c} = 0.075(4)$ or $\sigma_c = 70(4)$ MeV, is consistent with the direct determinations of ETM 16A [27] for $N_f = 2$ of $\sigma_c = 79(21)(^{12}_{8})$ MeV and χQCD 13A [43] for $N_f = 2+1$ of $\sigma_c = 94(31)$ MeV. MILC in MILC 12C [156] find $\langle N|\bar{c}c|N\rangle = 0.056(27)$ in the $\overline{\text{MS}}$ scheme at a scale of 2 GeV for $N_f = 2+1+1$ via the hybrid method. Considering the large uncertainty, this is consistent with the other results once multiplied by the charm quark mass.

10.4.5 Results for $g_T^{u,d,s}$

A compilation of recent results for the flavour-diagonal tensor charges $g_T^{u,d,s}$ for the proton in the $\overline{\text{MS}}$ scheme at 2 GeV is given in Tab. 68 and plotted in Fig. 46. Results for the neutron can be obtained by interchanging the u and d flavor indices. Only the PNDME 2+1+1 flavour calculations qualify for the global average.

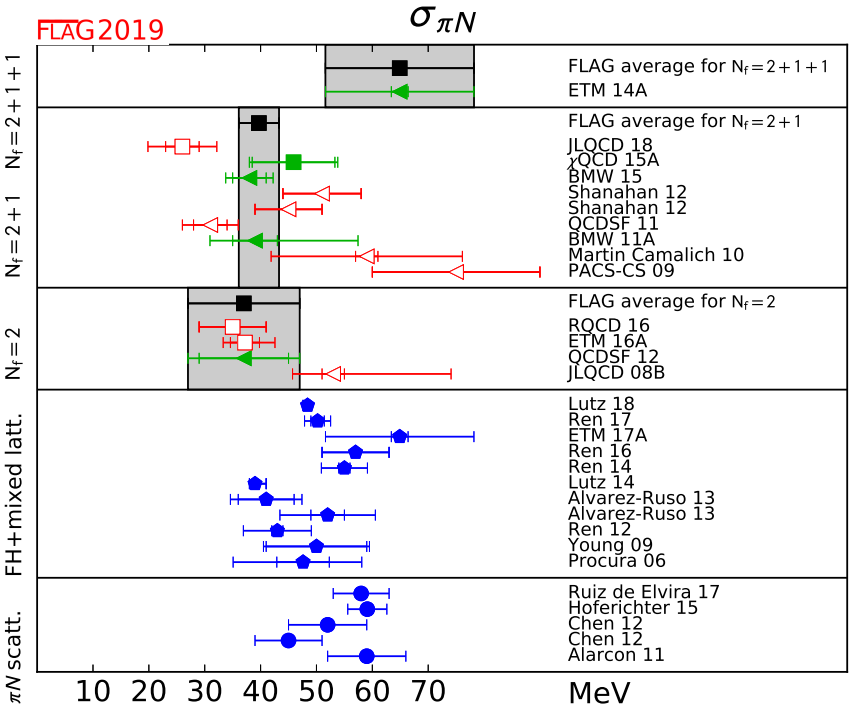

Figure 44: Lattice results and FLAG averages for the nucleon sigma term, $\sigma_{\pi N}$, for the $N_f = 2$, $2+1$, and $2+1+1$ flavour calculations. Determinations via the direct approach are indicated by squares and the Feynman-Hellmann method by triangles. Results from calculations which analyse more than one lattice data set within the Feynman-Hellmann approach [168, 174–182] are shown for comparison (pentagons) along with those from recent analyses of π-N scattering [153–155, 183] (circles).

The FLAG averages are the same as the PNDME 18B [36] results, which supersede the PNDME 16 [34] and the PNDME 15A [32] values:

$$N_f = 2+1+1: \qquad g_T^u = \quad 0.784(28)(10) \qquad \text{Ref. [36]}, \tag{401}$$

$$N_f = 2+1+1: \qquad g_T^d = -0.204(11)(10) \qquad \text{Ref. [36]}, \tag{402}$$

$$N_f = 2+1+1: \qquad g_T^s = -0.027(16) \qquad \text{Ref. [36]}. \tag{403}$$

The ensembles and the analysis strategy used in PNDME 18B is the same as described in Sec. 10.4.1 for $g_A^{u,d,s}$. The only difference for the tensor charges was that a one-state (constant) fit was used for the disconnected contributions as the data did not show significant excited-state contamination. The isovector renormalization constant, used for all three flavour diagonal tensor operators, was calculated on the lattice in the RI-SMOM scheme and converted to $\overline{\text{MS}}$ at 2 GeV using 2-loop perturbation theory. As discussed in Sec. 10.1.3, the difference between the singlet and isovector factors is expected to be small.

The JLQCD 18 [49] and ETM 17 calculations [30] were not considered for the final averages because they did not satisfy the criteria for the continuum extrapolation as already discussed

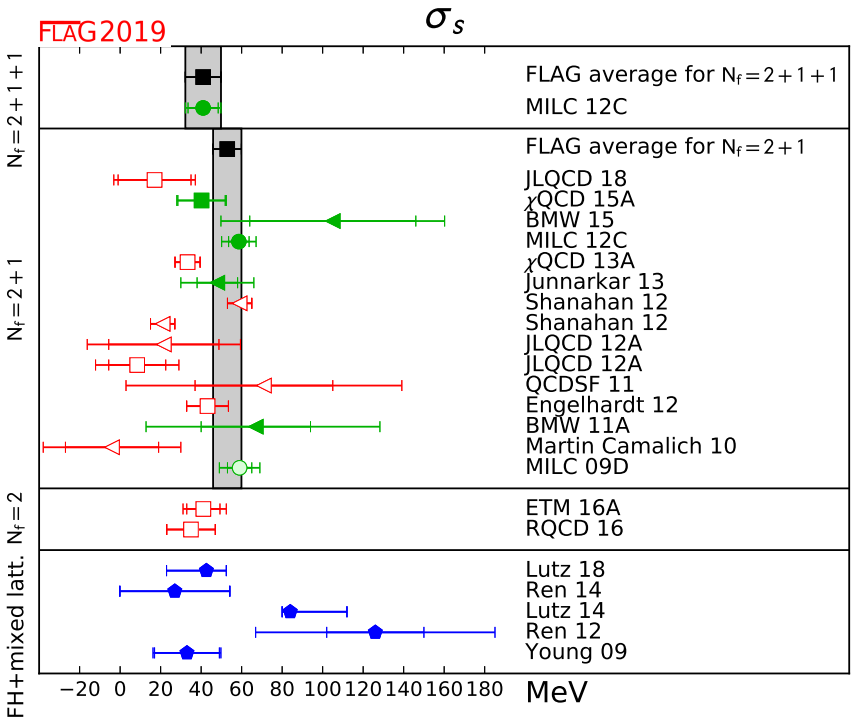

Figure 45: Lattice results and FLAG averages for σ_s for the $N_f = 2$, $2+1$, and $2+1+1$ flavour calculations. Determinations via the direct approach are indicated by squares, the Feynman-Hellmann method by triangles and the hybrid approach by circles. Results from calculations which analyse more than one lattice data set within the Feynman-Hellmann approach [175, 176, 178, 179, 182] are shown for comparison (pentagons).

in Sec. 10.4.1.

Collaboration	Ref.	N_f	publication status	continuum extrapolation	chiral extrapolation	finite volume	renormalization	excited states	g_T^u	g_T^d
PNDME 18B	[36]	2+1+1	P	★‡	★	★	★	★	0.784(28)(10)#	−0.204(11)(10)#
PNDME 16	[34]	2+1+1	A	○‡	★	★	★	★	0.792(42)#&	−0.194(14)#&
PNDME 15	[32, 33]	2+1+1	A	○‡	★	★	★	★	0.774(66)#	−0.233(28)#
JLQCD 18	[49]	2+1	A	■	○	○	★	★	0.85(3)(2)(7)	−0.24(2)(0)(2)
ETM 17	[30]	2	A	■	○	○	★	★	0.782(16)(2)(13)	−0.219(10)(2)(13)
									g_T^s	
PNDME 18B	[36]	2+1+1	P	★‡	★	★	★	★	−0.0027(16)#	
PNDME 15	[32, 33]	2+1+1	A	○‡	★	★	★	★	0.008(9)#	
JLQCD 18	[49]	2+1	A	■	○	○	★	★	−0.012(16)(8)	
ETM 17	[30]	2	A	■	○	○	★	★	−0.00319(69)(2)(22)	

‡ The rating takes into account that the action is not fully O(a) improved by requiring an additional lattice spacing.

Assumed that $Z_T^{n.s.} = Z_T^s$.

& Disconnected terms omitted.

Table 68: Overview of results for g_T^q.

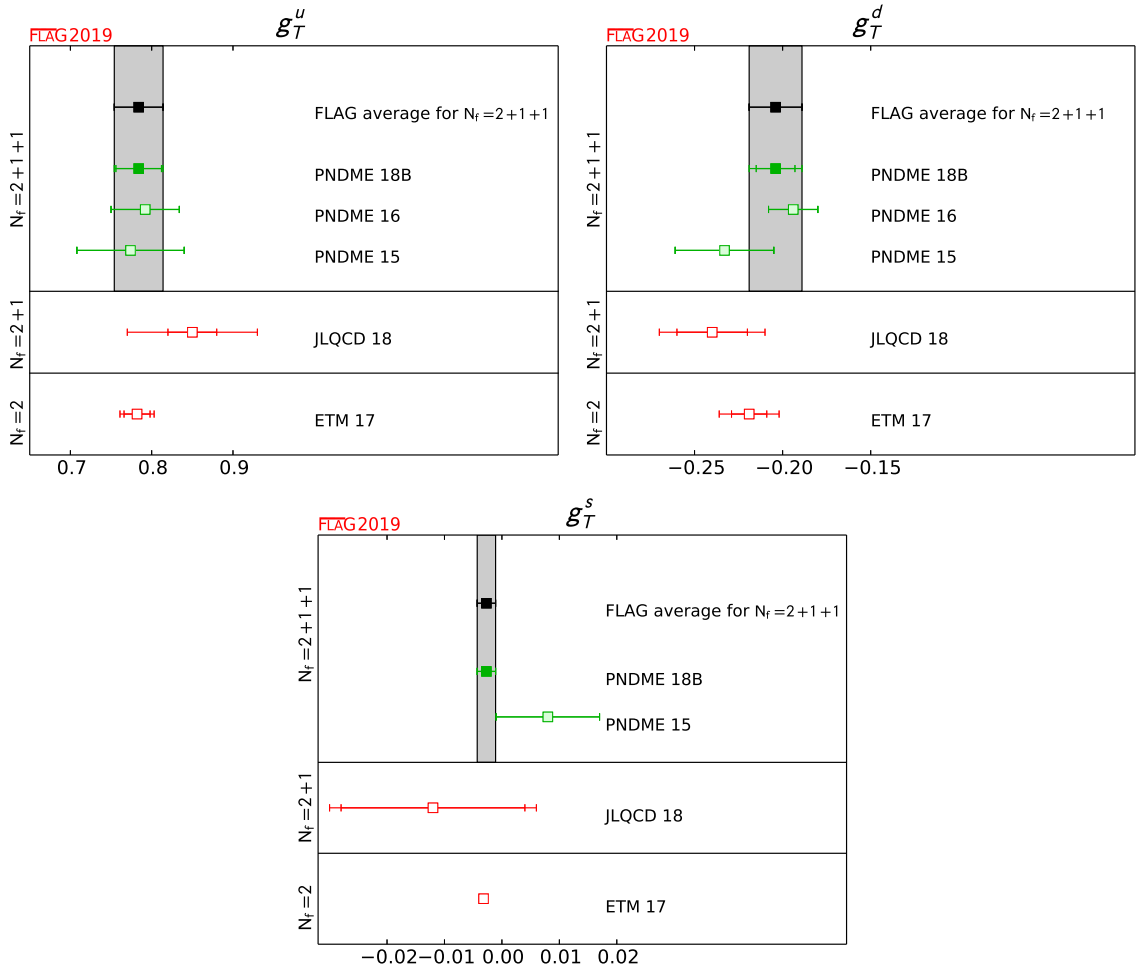

Figure 46: Lattice results and FLAG averages for $g_T^{u,d,s}$ for the $N_f = 2$, $2+1$, and $2+1+1$ flavour calculations.

References

[1] S. Syritsyn, *Review of Hadron Structure Calculations on a Lattice*, *PoS* **LATTICE2013** (2014) 009, [1403.4686].

[2] S. Capitani, M. Della Morte, D. Djukanovic, G. von Hippel, J. Hua, B. Jäger et al., *Nucleon electromagnetic form factors in two-flavor QCD*, *Phys. Rev.* **D92** (2015) 054511, [1504.04628].

[3] R. S. Sufian, Y.-B. Yang, A. Alexandru, T. Draper, J. Liang and K.-F. Liu, *Strange Quark Magnetic Moment of the Nucleon at the Physical Point*, *Phys. Rev. Lett.* **118** (2017) 042001, [1606.07075].

[4] R. Gupta, Y.-C. Jang, H.-W. Lin, B. Yoon and T. Bhattacharya, *Axial Vector Form Factors of the Nucleon from Lattice QCD*, *Phys. Rev.* **D96** (2017) 114503, [1705.06834].

[5] J. Green, N. Hasan, S. Meinel, M. Engelhardt, S. Krieg, J. Laeuchli et al., *Up, down, and strange nucleon axial form factors from lattice QCD*, *Phys. Rev.* **D95** (2017) 114502, [1703.06703].

[6] [CSSM/QCDSF/UKQCD 17] A. J. Chambers et al., *Electromagnetic form factors at large momenta from lattice QCD*, *Phys. Rev.* **D96** (2017) 114509, [1702.01513].

[7] C. Alexandrou, M. Constantinou, K. Hadjiyiannakou, K. Jansen, C. Kallidonis, G. Koutsou et al., *Nucleon electromagnetic form factors using lattice simulations at the physical point*, *Phys. Rev.* **D96** (2017) 034503, [1706.00469].

[8] C. Alexandrou, M. Constantinou, K. Hadjiyiannakou, K. Jansen, C. Kallidonis, G. Koutsou et al., *Strange nucleon electromagnetic form factors from lattice QCD*, *Phys. Rev.* **D97** (2018) 094504, [1801.09581].

[9] [PACS 18] K.-I. Ishikawa, Y. Kuramashi, S. Sasaki, N. Tsukamoto, A. Ukawa and T. Yamazaki, *Nucleon form factors on a large volume lattice near the physical point in 2+1 flavor QCD*, *Phys. Rev.* **D98** (2018) 074510, [1807.03974].

[10] H.-W. Lin et al., *Parton distributions and lattice QCD calculations: a community white paper*, *Prog. Part. Nucl. Phys.* **100** (2018) 107–160, [1711.07916].

[11] M. J. Savage, *Nuclear Physics from Lattice QCD*, *Prog. Part. Nucl. Phys.* **67** (2012) 140–152, [1110.5943].

[12] [NPLQCD 17] E. Chang, Z. Davoudi, W. Detmold, A. S. Gambhir, K. Orginos, M. J. Savage et al., *Scalar, Axial, and Tensor Interactions of Light Nuclei from Lattice QCD*, *Phys. Rev. Lett.* **120** (2018) 152002, [1712.03221].

[13] J. Carlson, S. Gandolfi, F. Pederiva, S. C. Pieper, R. Schiavilla, K. E. Schmidt et al., *Quantum Monte Carlo methods for nuclear physics*, *Rev. Mod. Phys.* **87** (2015) 1067, [1412.3081].

[14] M. L. Wagman, F. Winter, E. Chang, Z. Davoudi, W. Detmold, K. Orginos et al., *Baryon-Baryon Interactions and Spin-Flavor Symmetry from Lattice Quantum Chromodynamics*, *Phys. Rev.* **D96** (2017) 114510, [1706.06550].

[15] T. Iritani, *Two-baryon systems from HAL QCD method and the mirage in the temporal correlation of the direct method*, *EPJ Web Conf.* **175** (2018) 05008, [1710.06147].

[16] H. W. Hamber, E. Marinari, G. Parisi and C. Rebbi, *Considerations on Numerical Analysis of QCD*, *Nucl. Phys.* **B225** (1983) 475.

[17] G. P. Lepage, *The Analysis of Algorithms for Lattice Field Theory*, in *Boulder ASI 1989:97-120*, pp. 97–120, 1989.

[18] [QCDSF 06] A. A. Khan, M. Göckeler, P. Hägler, T. Hemmert, R. Horsley et al., *Axial coupling constant of the nucleon for two flavours of dynamical quarks in finite and infinite volume*, *Phys.Rev.* **D74** (2006) 094508, [hep-lat/0603028].

[19] [QCDSF 12] G. Bali, P. Bruns, S. Collins, M. Deka, B. Glasle et al., *Nucleon mass and sigma term from lattice QCD with two light fermion flavors*, *Nucl.Phys.* **B866** (2013) 1–25, [1206.7034].

[20] [QCDSF 13] R. Horsley, Y. Nakamura, A. Nobile, P. Rakow, G. Schierholz et al., *Nucleon axial charge and pion decay constant from two-flavor lattice QCD*, *Phys. Lett.* **B732** (2014) 41–48, [1302.2233].

[21] [Mainz 12] S. Capitani, M. Della Morte, G. von Hippel, B. Jager, A. Jüttner et al., *The nucleon axial charge from lattice QCD with controlled errors*, *Phys.Rev.* **D86** (2012) 074502, [1205.0180].

[22] [RQCD 14] G. S. Bali, S. Collins, B. Glässle, M. Göckeler, J. Najjar, R. H. Rödl et al., *Nucleon isovector couplings from $N_f = 2$ lattice QCD*, *Phys. Rev.* **D91** (2015) 054501, [1412.7336].

[23] [RQCD 16] G. S. Bali, S. Collins, D. Richtmann, A. Schäfer, W. Söldner and A. Sternbeck, *Direct determinations of the nucleon and pion σ terms at nearly physical quark masses*, *Phys. Rev.* **D93** (2016) 094504, [1603.00827].

[24] [Mainz 17] S. Capitani, M. Della Morte, D. Djukanovic, G. M. von Hippel, J. Hua, B. Jäger et al., *Iso-vector axial form factors of the nucleon in two-flavor lattice QCD*, *Int. J. Mod. Phys.* **A34** (2019) 1950009, [1705.06186].

[25] [PACS-CS 09] K.-I. Ishikawa et al., *SU(2) and SU(3) chiral perturbation theory analyses on baryon masses in 2+1 flavor lattice QCD*, *Phys. Rev.* **D80** (2009) 054502, [0905.0962].

[26] [ETM 15D] A. Abdel-Rehim et al., *Nucleon and pion structure with lattice QCD simulations at physical value of the pion mass*, *Phys. Rev.* **D92** (2015) 114513, [1507.04936].

[27] [ETM 16A] A. Abdel-Rehim, C. Alexandrou, M. Constantinou, K. Hadjiyiannakou, K. Jansen, C. Kallidonis et al., *Direct Evaluation of the Quark Content of Nucleons*

from Lattice QCD at the Physical Point, *Phys. Rev. Lett.* **116** (2016) 252001, [1601.01624].

[28] [ETM 17B] C. Alexandrou, M. Constantinou, K. Hadjiyiannakou, K. Jansen, C. Kallidonis, G. Koutsou et al., *Nucleon axial form factors using $N_f = 2$ twisted mass fermions with a physical value of the pion mass*, *Phys. Rev.* **D96** (2017) 054507, [1705.03399].

[29] [ETM 17C] C. Alexandrou, M. Constantinou, K. Hadjiyiannakou, K. Jansen, C. Kallidonis, G. Koutsou et al., *Nucleon Spin and Momentum Decomposition Using Lattice QCD Simulations*, *Phys. Rev. Lett.* **119** (2017) 142002, [1706.02973].

[30] [ETM 17] C. Alexandrou et al., *Nucleon scalar and tensor charges using lattice QCD simulations at the physical value of the pion mass*, *Phys. Rev.* **D95** (2017) 114514, [1703.08788].

[31] [PNDME 13] T. Bhattacharya, S. D. Cohen, R. Gupta, A. Joseph, H.-W. Lin and B. Yoon, *Nucleon Charges and Electromagnetic Form Factors from 2+1+1-Flavor Lattice QCD*, *Phys. Rev.* **D89** (2014) 094502, [1306.5435].

[32] [PNDME 15A] T. Bhattacharya, V. Cirigliano, S. Cohen, R. Gupta, A. Joseph, H.-W. Lin et al., *Iso-vector and Iso-scalar Tensor Charges of the Nucleon from Lattice QCD*, *Phys. Rev.* **D92** (2015) 094511, [1506.06411].

[33] [PNDME 15] T. Bhattacharya, V. Cirigliano, R. Gupta, H.-W. Lin and B. Yoon, *Neutron Electric Dipole Moment and Tensor Charges from Lattice QCD*, *Phys. Rev. Lett.* **115** (2015) 212002, [1506.04196].

[34] [PNDME 16] T. Bhattacharya, V. Cirigliano, S. Cohen, R. Gupta, H.-W. Lin and B. Yoon, *Axial, Scalar and Tensor Charges of the Nucleon from 2+1+1-flavor Lattice QCD*, *Phys. Rev.* **D94** (2016) 054508, [1606.07049].

[35] [CalLat 17] E. Berkowitz et al., *An accurate calculation of the nucleon axial charge with lattice QCD*, 1704.01114.

[36] [PNDME 18B] R. Gupta, B. Yoon, T. Bhattacharya, V. Cirigliano, Y.-C. Jang and H.-W. Lin, *Flavor diagonal tensor charges of the nucleon from (2+1+1)-flavor lattice QCD*, *Phys. Rev.* **D98** (2018) 091501, [1808.07597].

[37] [PNDME 18A] H.-W. Lin, R. Gupta, B. Yoon, Y.-C. Jang and T. Bhattacharya, *Quark contribution to the proton spin from 2+1+1-flavor lattice QCD*, *Phys. Rev.* **D98** (2018) 094512, [1806.10604].

[38] [PNDME 18] R. Gupta, Y.-C. Jang, B. Yoon, H.-W. Lin, V. Cirigliano and T. Bhattacharya, *Isovector Charges of the Nucleon from 2+1+1-flavor Lattice QCD*, *Phys. Rev.* **D98** (2018) 034503, [1806.09006].

[39] [CalLat 18] C. C. Chang et al., *A per-cent-level determination of the nucleon axial coupling from quantum chromodynamics*, *Nature* (2018) , [1805.12130].

[40] [RBC/UKQCD 08B] T. Yamazaki et al., *Nucleon axial charge in 2+1 flavor dynamical lattice QCD with domain wall fermions*, *Phys.Rev.Lett.* **100** (2008) 171602, [0801.4016].

[41] [RBC/UKQCD 09B] T. Yamazaki, Y. Aoki, T. Blum, H.-W. Lin, S. Ohta, S. Sasaki et al., *Nucleon form factors with 2+1 flavor dynamical domain-wall fermions*, *Phys. Rev.* **D79** (2009) 114505, [0904.2039].

[42] [RBC/UKQCD 10D] Y. Aoki, T. Blum, H.-W. Lin, S. Ohta, S. Sasaki, R. Tweedie et al., *Nucleon isovector structure functions in (2+1)-flavor QCD with domain wall fermions*, *Phys. Rev.* **D82** (2010) 014501, [1003.3387].

[43] [χQCD 13A] M. Gong et al., *Strangeness and charmness content of the nucleon from overlap fermions on 2+1-flavor domain-wall fermion configurations*, *Phys. Rev.* **D88** (2013) 014503, [1304.1194].

[44] [χQCD 15A] Y.-B. Yang, A. Alexandru, T. Draper, J. Liang and K.-F. Liu, *πN and strangeness sigma terms at the physical point with chiral fermions*, *Phys. Rev.* **D94** (2016) 054503, [1511.09089].

[45] [χQCD 15] M. Gong, Y.-B. Yang, J. Liang, A. Alexandru, T. Draper and K.-F. Liu, *Strange and charm quark spins from the anomalous Ward identity*, *Phys. Rev.* **D95** (2017) 114509, [1511.03671].

[46] [χQCD 18] J. Liang, Y.-B. Yang, T. Draper, M. Gong and K.-F. Liu, *Quark spins and Anomalous Ward Identity*, *Phys. Rev.* **D98** (2018) 074505, [1806.08366].

[47] [JLQCD 08B] H. Ohki, H. Fukaya, S. Hashimoto, T. Kaneko, H. Matsufuru, J. Noaki et al., *Nucleon sigma term and strange quark content from lattice QCD with exact chiral symmetry*, *Phys. Rev.* **D78** (2008) 054502, [0806.4744].

[48] [JLQCD 12A] H. Ohki, K. Takeda, S. Aoki, S. Hashimoto, T. Kaneko, H. Matsufuru et al., *Nucleon strange quark content from $N_f = 2 + 1$ lattice QCD with exact chiral symmetry*, *Phys. Rev.* **D87** (2013) 034509, [1208.4185].

[49] [JLQCD 18] N. Yamanaka, S. Hashimoto, T. Kaneko and H. Ohki, *Nucleon charges with dynamical overlap fermions*, *Phys. Rev.* **D98** (2018) 054516, [1805.10507].

[50] R. Babich, J. Brannick, R. C. Brower, M. A. Clark, T. A. Manteuffel, S. F. McCormick et al., *Adaptive multigrid algorithm for the lattice Wilson-Dirac operator*, *Phys. Rev. Lett.* **105** (2010) 201602, [1005.3043].

[51] M. Lüscher, *Deflation acceleration of lattice QCD simulations*, *JHEP* **12** (2007) 011, [0710.5417].

[52] G. S. Bali, S. Collins and A. Schafer, *Effective noise reduction techniques for disconnected loops in Lattice QCD*, *Comput. Phys. Commun.* **181** (2010) 1570–1583, [0910.3970].

[53] T. Blum, T. Izubuchi and E. Shintani, *New class of variance-reduction techniques using lattice symmetries*, *Phys. Rev.* **D88** (2013) 094503, [1208.4349].

[54] A. Stathopoulos, J. Laeuchli and K. Orginos, *Hierarchical probing for estimating the trace of the matrix inverse on toroidal lattices*, 1302.4018.

[55] A. S. Gambhir, A. Stathopoulos, K. Orginos, B. Yoon, R. Gupta and S. Syritsyn, *Algorithms for Disconnected Diagrams in Lattice QCD*, *PoS* **LATTICE2016** (2016) 265, [1611.01193].

[56] [LHPC 10] J. D. Bratt et al., *Nucleon structure from mixed action calculations using 2+1 flavors of asqtad sea and domain wall valence fermions*, *Phys.Rev.* **D82** (2010) 094502, [1001.3620].

[57] B. Yoon et al., *Controlling Excited-State Contamination in Nucleon Matrix Elements*, *Phys. Rev.* **D93** (2016) 114506, [1602.07737].

[58] T. A. DeGrand and S. Schaefer, *Improving meson two point functions in lattice QCD*, *Comput. Phys. Commun.* **159** (2004) 185–191, [hep-lat/0401011].

[59] L. Giusti, P. Hernandez, M. Laine, P. Weisz and H. Wittig, *Low-energy couplings of QCD from current correlators near the chiral limit*, *JHEP* **0404** (2004) 013, [hep-lat/0402002].

[60] R. Gupta, A. Patel, C. F. Baillie, G. Guralnik, G. W. Kilcup and S. R. Sharpe, *QCD With Dynamical Wilson Fermions*, *Phys. Rev.* **D40** (1989) 2072.

[61] C. Thron, S. Dong, K. Liu and H. Ying, *Pade - Z(2) estimator of determinants*, *Phys.Rev.* **D57** (1998) 1642–1653, [hep-lat/9707001].

[62] S. Bernardson, P. McCarty and C. Thron, *Monte Carlo methods for estimating linear combinations of inverse matrix entries in lattice QCD*, *Comput. Phys. Commun.* **78** (1993) 256–264.

[63] J. Foley et al., *Practical all-to-all propagators for lattice QCD*, *Comput. Phys. Commun.* **172** (2005) 145–162, [hep-lat/0505023].

[64] S. Güsken, U. Löw, K. H. Mütter, R. Sommer, A. Patel and K. Schilling, *Nonsinglet Axial Vector Couplings of the Baryon Octet in Lattice QCD*, *Phys. Lett.* **B227** (1989) 266–269.

[65] C. Alexandrou, F. Jegerlehner, S. Gusken, K. Schilling and R. Sommer, *B meson properties from lattice QCD*, *Phys. Lett.* **B256** (1991) 60–67.

[66] B. C. Tiburzi, *Time Dependence of Nucleon Correlation Functions in Chiral Perturbation Theory*, *Phys. Rev.* **D80** (2009) 014002, [0901.0657].

[67] O. Bär, *Multi-hadron-state contamination in nucleon observables from chiral perturbation theory*, *EPJ Web Conf.* **175** (2018) 01007, [1708.00380].

[68] O. Bär, *Nucleon-pion-state contribution in lattice calculations of the nucleon charges g_A, g_T and g_S*, *Phys. Rev.* **D94** (2016) 054505, [1606.09385].

[69] O. Bär, *Nucleon-pion-state contribution in lattice calculations of moments of parton distribution functions*, *Phys. Rev.* **D95** (2017) 034506, [1612.08336].

[70] M. T. Hansen and H. B. Meyer, *On the effect of excited states in lattice calculations of the nucleon axial charge*, *Nucl. Phys.* **B923** (2017) 558–587, [1610.03843].

[71] B. Yoon et al., *Isovector charges of the nucleon from 2+1-flavor QCD with clover fermions*, *Phys. Rev.* **D95** (2017) 074508, [1611.07452].

[72] L. Maiani, G. Martinelli, M. L. Paciello and B. Taglienti, *Scalar Densities and Baryon Mass Differences in Lattice QCD With Wilson Fermions*, *Nucl. Phys.* **B293** (1987) 420.

[73] S. J. Dong, K. F. Liu and A. G. Williams, *Lattice calculation of the strangeness magnetic moment of the nucleon*, *Phys. Rev.* **D58** (1998) 074504, [hep-ph/9712483].

[74] S. Capitani, B. Knippschild, M. Della Morte and H. Wittig, *Systematic errors in extracting nucleon properties from lattice QCD*, *PoS* **LATTICE2010** (2010) 147, [1011.1358].

[75] J. Bulava, M. Donnellan and R. Sommer, *On the computation of hadron-to-hadron transition matrix elements in lattice QCD*, *JHEP* **01** (2012) 140, [1108.3774].

[76] S. Güsken, K. Schilling, R. Sommer, K. H. Mütter and A. Patel, *Mass Splittings in the Baryon Octet and the Nucleon σ Term in Lattice QCD*, *Phys. Lett.* **B212** (1988) 216–220.

[77] R. Sommer, *Current matrix elements with quenched Wilson fermions*, *Nucl. Phys. Proc. Suppl.* **17** (1990) 513–517.

[78] C. Bouchard, C. C. Chang, T. Kurth, K. Orginos and A. Walker-Loud, *On the Feynman-Hellmann Theorem in Quantum Field Theory and the Calculation of Matrix Elements*, *Phys. Rev.* **D96** (2017) 014504, [1612.06963].

[79] [CSSM/QCDSF/UKQCD 14] A. J. Chambers et al., *Feynman-Hellmann approach to the spin structure of hadrons*, *Phys. Rev.* **D90** (2014) 014510, [1405.3019].

[80] A. J. Chambers et al., *Disconnected contributions to the spin of the nucleon*, *Phys. Rev.* **D92** (2015) 114517, [1508.06856].

[81] B. J. Owen, J. Dragos, W. Kamleh, D. B. Leinweber, M. S. Mahbub, B. J. Menadue et al., *Variational Approach to the Calculation of gA*, *Phys. Lett.* **B723** (2013) 217–223, [1212.4668].

[82] G. Fox, R. Gupta, O. Martin and S. Otto, *Monte Carlo Estimates of the Mass Gap of the O(2) and O(3) Spin Models in (1+1)-dimensions*, *Nucl. Phys.* **B205** (1982) 188–220.

[83] C. Michael, *Adjoint Sources in Lattice Gauge Theory*, *Nucl. Phys.* **B259** (1985) 58–76.

[84] M. Lüscher and U. Wolff, *How to Calculate the Elastic Scattering Matrix in Two-dimensional Quantum Field Theories by Numerical Simulation*, *Nucl. Phys.* **B339** (1990) 222–252.

[85] B. Blossier, M. Della Morte, G. von Hippel, T. Mendes and R. Sommer, *On the generalized eigenvalue method for energies and matrix elements in lattice field theory*, *JHEP* **04** (2009) 094, [0902.1265].

[86] J. Dragos, R. Horsley, W. Kamleh, D. B. Leinweber, Y. Nakamura, P. E. L. Rakow et al., *Nucleon matrix elements using the variational method in lattice QCD*, *Phys. Rev.* **D94** (2016) 074505, [1606.03195].

[87] K. Jansen, C. Liu, M. Luscher, H. Simma, S. Sint, R. Sommer et al., *Nonperturbative renormalization of lattice QCD at all scales*, *Phys. Lett.* **B372** (1996) 275–282, [hep-lat/9512009].

[88] M. Lüscher, S. Sint, R. Sommer and P. Weisz, *Chiral symmetry and O(a) improvement in lattice QCD*, *Nucl. Phys.* **B478** (1996) 365–400, [hep-lat/9605038].

[89] [RQCD 16A] G. S. Bali, E. E. Scholz, J. Simeth and W. Sldner, *Lattice simulations with $N_f = 2 + 1$ improved Wilson fermions at a fixed strange quark mass*, *Phys. Rev.* **D94** (2016) 074501, [1606.09039].

[90] A. Gerardin, T. Harris and H. B. Meyer, *Non-perturbative renormalization and $O(a)$-improvement of the non-singlet vector current with $N_{\rm f} = 2 + 1$ Wilson fermions and tree-level Symanzik improved gauge action*, *Phys. Rev.* **D99** (2019) 014519, [1811.08209].

[91] R. Frezzotti and G. C. Rossi, *Chirally improving Wilson fermions. I: O(a) improvement*, *JHEP* **08** (2004) 007, [hep-lat/0306014].

[92] R. Frezzotti and G. C. Rossi, *Twisted mass lattice QCD with mass nondegenerate quarks*, *Nucl. Phys. Proc. Suppl.* **128** (2004) 193–202, [hep-lat/0311008].

[93] S. Capitani, M. Göckeler, R. Horsley, H. Perlt, P. E. L. Rakow, G. Schierholz et al., *Renormalization and off-shell improvement in lattice perturbation theory*, *Nucl. Phys.* **B593** (2001) 183–228, [hep-lat/0007004].

[94] T. Bhattacharya, R. Gupta, W. Lee, S. R. Sharpe and J. M. S. Wu, *Improved bilinears in lattice QCD with non-degenerate quarks*, *Phys. Rev.* **D73** (2006) 034504, [hep-lat/0511014].

[95] M. Bochicchio, L. Maiani, G. Martinelli, G. C. Rossi and M. Testa, *Chiral symmetry on the lattice with Wilson fermions*, *Nucl.Phys.* **B262** (1985) 331.

[96] G. Martinelli, C. Pittori, C. T. Sachrajda, M. Testa and A. Vladikas, *A general method for nonperturbative renormalization of lattice operators*, *Nucl. Phys.* **B445** (1995) 81–108, [hep-lat/9411010].

[97] [RBC/UKQCD 14B] T. Blum et al., *Domain wall QCD with physical quark masses*, *Phys. Rev.* **D93** (2016) 074505, [1411.7017].

[98] S. Sint and P. Weisz, *Further results on O(a) improved lattice QCD to one loop order of perturbation theory*, *Nucl. Phys.* **B502** (1997) 251–268, [hep-lat/9704001].

[99] Y. Taniguchi and A. Ukawa, *Perturbative calculation of improvement coefficients to O(g**2a) for bilinear quark operators in lattice QCD*, *Phys. Rev.* **D58** (1998) 114503, [hep-lat/9806015].

[100] P. Korcyl and G. S. Bali, *Non-perturbative determination of improvement coefficients using coordinate space correlators in $N_f = 2 + 1$ lattice QCD*, *Phys. Rev.* **D95** (2017) 014505, [1607.07090].

[101] M. Constantinou, M. Hadjiantonis, H. Panagopoulos and G. Spanoudes, *Singlet versus nonsinglet perturbative renormalization of fermion bilinears*, *Phys. Rev.* **D94** (2016) 114513, [1610.06744].

[102] G. S. Bali, S. Collins, M. Göckeler, S. Piemonte and A. Sternbeck, *Non-perturbative renormalization of flavor singlet quark bilinear operators in lattice QCD*, *PoS* **LATTICE2016** (2016) 187, [1703.03745].

[103] S. Dinter, V. Drach, R. Frezzotti, G. Herdoiza, K. Jansen and G. Rossi, *Sigma terms and strangeness content of the nucleon with $N_f = 2 + 1 + 1$ twisted mass fermions*, *JHEP* **08** (2012) 037, [1202.1480].

[104] [ALPHA 12] P. Fritzsch, F. Knechtli, B. Leder, M. Marinkovic, S. Schaefer et al., *The strange quark mass and the Λ parameter of two flavor QCD*, *Nucl.Phys.* **B865** (2012) 397–429, [1205.5380].

[105] [BMW 12A] S. Borsanyi, S. Dürr, Z. Fodor, C. Hoelbling, S. D. Katz et al., *High-precision scale setting in lattice QCD*, *JHEP* **1209** (2012) 010, [1203.4469].

[106] E. E. Jenkins and A. V. Manohar, *Baryon chiral perturbation theory using a heavy fermion Lagrangian*, *Phys. Lett.* **B255** (1991) 558–562.

[107] T. N. Truong, *Chiral Perturbation Theory and Final State Theorem*, *Phys. Rev. Lett.* **61** (1988) 2526.

[108] A. Walker-Loud et al., *Light hadron spectroscopy using domain wall valence quarks on an Asqtad sea*, *Phys. Rev.* **D79** (2009) 054502, [0806.4549].

[109] A. Torok, S. R. Beane, W. Detmold, T. C. Luu, K. Orginos, A. Parreno et al., *Meson-Baryon Scattering Lengths from Mixed-Action Lattice QCD*, *Phys. Rev.* **D81** (2010) 074506, [0907.1913].

[110] E. E. Jenkins, A. V. Manohar, J. W. Negele and A. Walker-Loud, *A Lattice Test of 1/N(c) Baryon Mass Relations*, *Phys. Rev.* **D81** (2010) 014502, [0907.0529].

[111] A. Walker-Loud, *Evidence for non-analytic light quark mass dependence in the baryon spectrum*, *Phys. Rev.* **D86** (2012) 074509, [1112.2658].

[112] V. Bernard, N. Kaiser, J. Kambor and U. G. Meissner, *Chiral structure of the nucleon*, *Nucl. Phys.* **B388** (1992) 315–345.

[113] S. R. Beane and M. J. Savage, *Baryon axial charge in a finite volume*, *Phys. Rev.* **D70** (2004) 074029, [hep-ph/0404131].

[114] R. E. Kass and A. E. Raftery, *Bayes factors*, *Journal of the American Statistical Association* **90** (1995) 773–795, [https://amstat.tandfonline.com/doi/pdf/10.1080/01621459.1995.10476572].

[115] H. Akaike, *A new look at the statistical model identification*, *IEEE Transactions on Automatic Control* **19** (Dec, 1974) 716–723.

[116] M. Schmelling, *Averaging correlated data*, *Phys.Scripta* **51** (1995) 676–679.

[117] T. Bhattacharya, V. Cirigliano, S. D. Cohen, A. Filipuzzi, M. Gonzalez-Alonso et al., *Probing Novel Scalar and Tensor Interactions from (Ultra)Cold Neutrons to the LHC*, *Phys.Rev.* **D85** (2012) 054512, [1110.6448].

[118] UCNA collaboration, M. Mendenhall et al., *Precision measurement of the neutron β-decay asymmetry*, *Phys.Rev.* **C87** (2013) 032501, [1210.7048].

[119] UCNA collaboration, M. A. P. Brown et al., *New result for the neutron β-asymmetry parameter A_0 from UCNA*, *Phys. Rev.* **C97** (2018) 035505, [1712.00884].

[120] D. Mund, B. Maerkisch, M. Deissenroth, J. Krempel, M. Schumann, H. Abele et al., *Determination of the Weak Axial Vector Coupling from a Measurement of the Beta-Asymmetry Parameter A in Neutron Beta Decay*, *Phys. Rev. Lett.* **110** (2013) 172502, [1204.0013].

[121] M. Ademollo and R. Gatto, *Nonrenormalization Theorem for the Strangeness Violating Vector Currents*, *Phys.Rev.Lett.* **13** (1964) 264–265.

[122] J. F. Donoghue and D. Wyler, *Isospin breaking and the precise determination of V_{ud}*, *Phys.Lett.* **B241** (1990) 243.

[123] R. Alarcon et al., *Precise Measurement of Neutron Decay Parameters*, 2007.

[124] W. Wilburn et al., *Measurement of the neutrino-spin correlation Parameter b in neutron decay using ultracold neutrons*, *Rev. Mex. Fis.* **Suppl. 55** (2009) 119.

[125] Nab collaboration, D. Pocanic et al., *Nab: Measurement Principles, Apparatus and Uncertainties*, *Nucl.Instrum.Meth.* **A611** (2009) 211–215, [0810.0251].

[126] M. Gonzalez-Alonso and J. Martin Camalich, *Isospin breaking in the nucleon mass and the sensitivity of β decays to new physics*, *Phys. Rev. Lett.* **112** (2014) 042501, [1309.4434].

[127] [FLAG 13] S. Aoki, Y. Aoki, C. Bernard, T. Blum, G. Colangelo et al., *Review of lattice results concerning low-energy particle physics*, *Eur.Phys.J.* **C74** (2014) 2890, [1310.8555].

[128] J. Dudek et al., *Physics Opportunities with the 12 GeV Upgrade at Jefferson Lab*, *Eur. Phys. J.* **A48** (2012) 187, [1208.1244].

[129] Z. Ye, N. Sato, K. Allada, T. Liu, J.-P. Chen, H. Gao et al., *Unveiling the nucleon tensor charge at Jefferson Lab: A study of the SoLID case*, *Phys. Lett.* **B767** (2017) 91–98, [1609.02449].

[130] H.-W. Lin, W. Melnitchouk, A. Prokudin, N. Sato and H. Shows, *First Monte Carlo Global Analysis of Nucleon Transversity with Lattice QCD Constraints*, *Phys. Rev. Lett.* **120** (2018) 152502, [1710.09858].

[131] M. Radici and A. Bacchetta, *First Extraction of Transversity from a Global Analysis of Electron-Proton and Proton-Proton Data*, *Phys. Rev. Lett.* **120** (2018) 192001, [1802.05212].

[132] [Mainz 18] K. Ottnad, T. Harris, H. Meyer, G. von Hippel, J. Wilhelm and H. Wittig, *Nucleon charges and quark momentum fraction with $N_f = 2 + 1$ Wilson fermions*, in *Proceedings, 36th International Symposium on Lattice Field Theory (Lattice 2018): East Lansing, MI, United States, July 22-28, 2018*, vol. LATTICE2018, p. 129, 2018. 1809.10638. DOI.

[133] [LHPC 12A] J. R. Green, M. Engelhardt, S. Krieg, J. W. Negele, A. V. Pochinsky and S. N. Syritsyn, *Nucleon Structure from Lattice QCD Using a Nearly Physical Pion Mass*, *Phys. Lett.* **B734** (2014) 290–295, [1209.1687].

[134] [LHPC 05] R. G. Edwards et al., *The nucleon axial charge in full lattice QCD*, *Phys. Rev. Lett.* **96** (2006) 052001, [hep-lat/0510062].

[135] [RBC 08] H.-W. Lin, T. Blum, S. Ohta, S. Sasaki and T. Yamazaki, *Nucleon structure with two flavors of dynamical domain-wall fermions*, *Phys.Rev.* **D78** (2008) 014505, [0802.0863].

[136] [LHP/RBC/UKQCD 18] S. Ohta, *Nucleon isovector axial charge in $2 + 1$-flavor domain-wall QCD with physical mass*, in *36th International Symposium on Lattice Field Theory (Lattice 2018) East Lansing, MI, United States, July 22-28, 2018*, vol. LATTICE2018, p. 128, 2018. 1810.09737. DOI.

[137] [LHPC 12] J. R. Green, J. W. Negele, A. V. Pochinsky, S. N. Syritsyn, M. Engelhardt and S. Krieg, *Nucleon Scalar and Tensor Charges from Lattice QCD with Light Wilson Quarks*, *Phys. Rev.* **D86** (2012) 114509, [1206.4527].

[138] M. Radici, A. Courtoy, A. Bacchetta and M. Guagnelli, *Improved extraction of valence transversity distributions from inclusive dihadron production*, *JHEP* **05** (2015) 123, [1503.03495].

[139] Z.-B. Kang, A. Prokudin, P. Sun and F. Yuan, *Extraction of Quark Transversity Distribution and Collins Fragmentation Functions with QCD Evolution*, *Phys. Rev.* **D93** (2016) 014009, [1505.05589].

[140] Z.-B. Kang, *private communication, Jun. 2015.*

[141] G. R. Goldstein, J. O. Gonzalez Hernandez and S. Liuti, *Flavor dependence of chiral odd generalized parton distributions and the tensor charge from the analysis of combined π^0 and η exclusive electroproduction data*, 1401.0438.

[142] M. Pitschmann, C.-Y. Seng, C. D. Roberts and S. M. Schmidt, *Nucleon tensor charges and electric dipole moments*, *Phys. Rev.* **D91** (2015) 074004, [1411.2052].

[143] M. A. Shifman, A. I. Vainshtein and V. I. Zakharov, *Remarks on Higgs Boson Interactions with Nucleons*, *Phys. Lett.* **78B** (1978) 443–446.

[144] K. G. Chetyrkin, B. A. Kniehl and M. Steinhauser, *Decoupling relations to O (alpha-s**3) and their connection to low-energy theorems*, *Nucl. Phys.* **B510** (1998) 61–87, [hep-ph/9708255].

[145] R. J. Hill and M. P. Solon, *Standard Model anatomy of WIMP dark matter direct detection II: QCD analysis and hadronic matrix elements*, *Phys. Rev.* **D91** (2015) 043505, [1409.8290].

[146] European Muon collaboration, J. Ashman et al., *A Measurement of the Spin Asymmetry and Determination of the Structure Function g(1) in Deep Inelastic Muon-Proton Scattering*, *Phys. Lett.* **B206** (1988) 364.

[147] X.-D. Ji, *Gauge-Invariant Decomposition of Nucleon Spin*, *Phys. Rev. Lett.* **78** (1997) 610–613, [hep-ph/9603249].

[148] R. L. Jaffe and A. Manohar, *The G(1) Problem: Fact and Fantasy on the Spin of the Proton*, *Nucl. Phys.* **B337** (1990) 509–546.

[149] M. Pospelov and A. Ritz, *Electric dipole moments as probes of new physics*, *Annals Phys.* **318** (2005) 119–169, [hep-ph/0504231].

[150] C. Baker, D. Doyle, P. Geltenbort, K. Green, M. van der Grinten et al., *An Improved experimental limit on the electric dipole moment of the neutron*, *Phys.Rev.Lett.* **97** (2006) 131801, [hep-ex/0602020].

[151] C.-Y. Seng, *Reexamination of The Standard Model Nucleon Electric Dipole Moment*, *Phys. Rev.* **C91** (2015) 025502, [1411.1476].

[152] M. Engelhardt, *Strange quark contributions to nucleon mass and spin from lattice QCD*, *Phys. Rev.* **D86** (2012) 114510, [1210.0025].

[153] J. M. Alarcon, J. Martin Camalich and J. A. Oller, *The chiral representation of the πN scattering amplitude and the pion-nucleon sigma term*, *Phys. Rev.* **D85** (2012) 051503, [1110.3797].

[154] Y.-H. Chen, D.-L. Yao and H. Q. Zheng, *Analyses of pion-nucleon elastic scattering amplitudes up to $O(p^4)$ in extended-on-mass-shell subtraction scheme*, *Phys. Rev.* **D87** (2013) 054019, [1212.1893].

[155] M. Hoferichter, J. Ruiz de Elvira, B. Kubis and U.-G. Meissner, *High-Precision Determination of the Pion-Nucleon σ Term from Roy-Steiner Equations*, *Phys. Rev. Lett.* **115** (2015) 092301, [1506.04142].

[156] [MILC 12C] W. Freeman and D. Toussaint, *Intrinsic strangeness and charm of the nucleon using improved staggered fermions*, *Phys. Rev.* **D88** (2013) 054503, [1204.3866].

[157] [MILC 09D] D. Toussaint and W. Freeman, *The Strange quark condensate in the nucleon in 2+1 flavor QCD*, *Phys. Rev. Lett.* **103** (2009) 122002, [0905.2432].

[158] [JLQCD 10A] K. Takeda, S. Aoki, S. Hashimoto, T. Kaneko, J. Noaki and T. Onogi, *Nucleon strange quark content from two-flavor lattice QCD with exact chiral symmetry*, *Phys. Rev.* **D83** (2011) 114506, [1011.1964].

[159] [HPQCD 05] Q. Mason, H. D. Trottier, R. Horgan, C. T. H. Davies and G. P. Lepage, *High-precision determination of the light-quark masses from realistic lattice QCD*, *Phys. Rev.* **D73** (2006) 114501, [hep-ph/0511160].

[160] C. McNeile, A. Bazavov, C. T. H. Davies, R. J. Dowdall, K. Hornbostel, G. P. Lepage et al., *Direct determination of the strange and light quark condensates from full lattice QCD*, *Phys. Rev.* **D87** (2013) 034503, [1211.6577].

[161] [ETM 14A] C. Alexandrou, V. Drach, K. Jansen, C. Kallidonis and G. Koutsou, *Baryon spectrum with $N_f = 2 + 1 + 1$ twisted mass fermions*, *Phys. Rev.* **D90** (2014) 074501, [1406.4310].

[162] [BMW 15] S. Dürr et al., *Lattice computation of the nucleon scalar quark contents at the physical point*, *Phys. Rev. Lett.* **116** (2016) 172001, [1510.08013].

[163] P. Junnarkar and A. Walker-Loud, *Scalar strange content of the nucleon from lattice QCD*, *Phys. Rev.* **D87** (2013) 114510, [1301.1114].

[164] P. E. Shanahan, A. W. Thomas and R. D. Young, *Sigma terms from an SU(3) chiral extrapolation*, *Phys. Rev.* **D87** (2013) 074503, [1205.5365].

[165] [QCDSF/UKQCD 11] R. Horsley, Y. Nakamura, H. Perlt, D. Pleiter, P. E. L. Rakow, G. Schierholz et al., *Hyperon sigma terms for 2+1 quark flavours*, *Phys. Rev.* **D85** (2012) 034506, [1110.4971].

[166] [BMW 11A] S. Dürr et al., *Sigma term and strangeness content of octet baryons*, *Phys. Rev.* **D85** (2012) 014509, [1109.4265].

[167] J. Martin Camalich, L. S. Geng and M. J. Vicente Vacas, *The lowest-lying baryon masses in covariant SU(3)-flavor chiral perturbation theory*, *Phys. Rev.* **D82** (2010) 074504, [1003.1929].

[168] [ETM 17A] C. Alexandrou and C. Kallidonis, *Low-lying baryon masses using $N_f = 2$ twisted mass clover-improved fermions directly at the physical pion mass*, *Phys. Rev.* **D96** (2017) 034511, [1704.02647].

[169] C. Kallidonis, *private communication, Nov. 2018.*

[170] [ETM 09H] C. Alexandrou, R. Baron, J. Carbonell, V. Drach, P. Guichon, K. Jansen et al., *Low-lying baryon spectrum with two dynamical twisted mass fermions*, *Phys. Rev.* **D80** (2009) 114503, [0910.2419].

[171] [BMW 08] S. Dürr et al., *Ab-initio determination of light hadron masses*, *Science* **322** (2008) 1224–1227, [0906.3599].

[172] A. Crivellin, M. Hoferichter and M. Procura, *Accurate evaluation of hadronic uncertainties in spin-independent WIMP-nucleon scattering: Disentangling two- and three-flavor effects*, *Phys. Rev.* **D89** (2014) 054021, [1312.4951].

[173] [PACS-CS 08] S. Aoki et al., *2+1 flavor lattice QCD toward the physical point*, *Phys. Rev.* **D79** (2009) 034503, [0807.1661].

[174] M. Procura, B. U. Musch, T. Wollenweber, T. R. Hemmert and W. Weise, *Nucleon mass: From lattice QCD to the chiral limit*, *Phys. Rev.* **D73** (2006) 114510, [hep-lat/0603001].

[175] R. D. Young and A. W. Thomas, *Octet baryon masses and sigma terms from an SU(3) chiral extrapolation*, *Phys. Rev.* **D81** (2010) 014503, [0901.3310].

[176] X. L. Ren, L. S. Geng, J. Martin Camalich, J. Meng and H. Toki, *Octet baryon masses in next-to-next-to-next-to-leading order covariant baryon chiral perturbation theory*, *JHEP* **12** (2012) 073, [1209.3641].

[177] L. Alvarez-Ruso, T. Ledwig, J. Martin Camalich and M. J. Vicente-Vacas, *Nucleon mass and pion-nucleon sigma term from a chiral analysis of lattice QCD data*, *Phys. Rev.* **D88** (2013) 054507, [1304.0483].

[178] M. F. M. Lutz, R. Bavontaweepanya, C. Kobdaj and K. Schwarz, *Finite volume effects in the chiral extrapolation of baryon masses*, *Phys. Rev.* **D90** (2014) 054505, [1401.7805].

[179] X.-L. Ren, L.-S. Geng and J. Meng, *Scalar strangeness content of the nucleon and baryon sigma terms*, *Phys. Rev.* **D91** (2015) 051502, [1404.4799].

[180] X.-L. Ren, L. Alvarez-Ruso, L.-S. Geng, T. Ledwig, J. Meng and M. J. Vicente Vacas, *Consistency between SU(3) and SU(2) covariant baryon chiral perturbation theory for the nucleon mass*, *Phys. Lett.* **B766** (2017) 325–333, [1606.03820].

[181] X.-Z. Ling, X.-L. Ren and L.-S. Geng, *Pion-nucleon sigma term revisited in covariant baryon chiral perturbation theory*, *Phys. Lett.* **B783** (2018) 7–12, [1710.07164].

[182] M. F. M. Lutz, Y. Heo and X.-Y. Guo, *On the convergence of the chiral expansion for the baryon ground-state masses*, *Nucl. Phys.* **A977** (2018) 146–207, [1801.06417].

[183] J. Ruiz de Elvira, M. Hoferichter, B. Kubis and U.-G. Meissner, *Extracting the σ-term from low-energy pion-nucleon scattering*, *J. Phys.* **G45** (2018) 024001, [1706.01465].